JOURNAL OF GEOPHYSICAL RESEARCH, VOL. 111, B11303, doi:10.1029/2005JB004240, 2006

Imaging the transition from Aleutian subduction to Yakutat collision in central Alaska, with local earthquakes and active source data

Donna Eberhart-Phillips,[1,2] Douglas H. Christensen,[3] Thomas M. Brocher,[4] Roger Hansen,[3] Natalia A. Ruppert,[3] Peter J. Haeussler,[1] and Geoffrey A. Abers[5]

Received 22 December 2005; revised 24 May 2006; accepted 21 June 2006; published 8 November 2006.

[1] In southern and central Alaska the subduction and active volcanism of the Aleutian subduction zone give way to a broad plate boundary zone with mountain building and strike-slip faulting, where the Yakutat terrane joins the subducting Pacific plate. The interplay of these tectonic elements can be best understood by considering the entire region in three dimensions. We image three-dimensional seismic velocity using abundant local earthquakes, supplemented by active source data. Crustal low-velocity correlates with basins. The Denali fault zone is a dominant feature with a change in crustal thickness across the fault. A relatively high-velocity subducted slab and a low-velocity mantle wedge are observed, and high V_p/V_s beneath the active volcanic systems, which indicates focusing of partial melt. North of Cook Inlet, the subducted Yakutat slab is characterized by a thick low-velocity, high-V_p/V_s crust. High-velocity material above the Yakutat slab may represent a residual older slab, which inhibits vertical flow of Yakutat subduction fluids. Alternate lateral flow allows Yakutat subduction fluids to contribute to Cook Inlet volcanism and the Wrangell volcanic field. The apparent northeast edge of the subducted Yakutat slab is southwest of the Wrangell volcanics, which have adakitic composition consistent with melting of this Yakutat slab edge. In the mantle, the Yakutat slab is subducting with the Pacific plate, while at shallower depths the Yakutat slab overthrusts the shallow Pacific plate along the Transition fault. This region of crustal doubling within the shallow slab is associated with extremely strong plate coupling and the primary asperity of the M_w 9.2 great 1964 earthquake.

Citation: Eberhart-Phillips, D., D. H. Christensen, T. M. Brocher, R. Hansen, N. A. Ruppert, P. J. Haeussler, and G. A. Abers (2006), Imaging the transition from Aleutian subduction to Yakutat collision in central Alaska, with local earthquakes and active source data, *J. Geophys. Res.*, *111*, B11303, doi:10.1029/2005JB004240.

1. Introduction

[2] Southern Alaska, at the north end of the subducting Pacific plate, has been the end of the road for accreting displaced terranes since the Cretaceous (Figure 1) [e.g., *Plafker and Berg*, 1994]. A trench bounds the Pacific plate on the north, and strike-slip faults on the east, leading to a ''corner'' geometry. The accreting Yakutat terrane, or microplate, currently occupies this corner [*Plafker*, 1987] and is bound by right-lateral transform faults on the east and a subduction zone on the west (Figure 2). This area is associated with a gap in volcanism between the Aleutian arc and the Wrangell volcanoes. The subducted extent of the Yakutat terrane and its relation to the Pacific plate slab are important targets for tomographic study, as are the bending of the subducted Pacific plate in central Alaska [*Ratchkovski and Hansen*, 2002], and variability in the upper mantle of the Yakutat-Aleutian region related to patterns of volcanism.

[3] The M_w 9.2 great Alaska earthquake of 1964 highlights the seismic potential of the Aleutian megathrust in central Alaska. The 800-km-long rupture zone includes extreme variation in plate coupling [*Zweck et al.*, 2002], with the central rupture section being very weakly coupled and the hypocentral area in Prince William Sound being very strongly coupled. For consideration of earthquake potential and rupture scenarios in subduction systems, it is crucial to understand factors that may result in weak coupling and in strong coupling.

[4] In this paper, we examine the subduction zone as a whole from the offshore trench to 200-km depth, and across the plate boundary region from the Alaska Peninsula to northeast of the Denali fault. This large-scale study allows interpretation of the combined features of this end zone of Aleutian subduction, and provides input for future fully three-dimensional (3-D) finite element models. The large

[1] U.S. Geological Survey, Anchorage, Alaska, USA.
[2] GNS Science, Dunedin, New Zealand.
[3] Geophysical Institute, University of Alaska, Fairbanks, Alaska, USA.
[4] U.S. Geological Survey, Menlo Park, California, USA.
[5] Department of Earth Sciences, Boston University, Boston, Massachusetts, USA.

0148-0227/06/2005JB004240$09.00

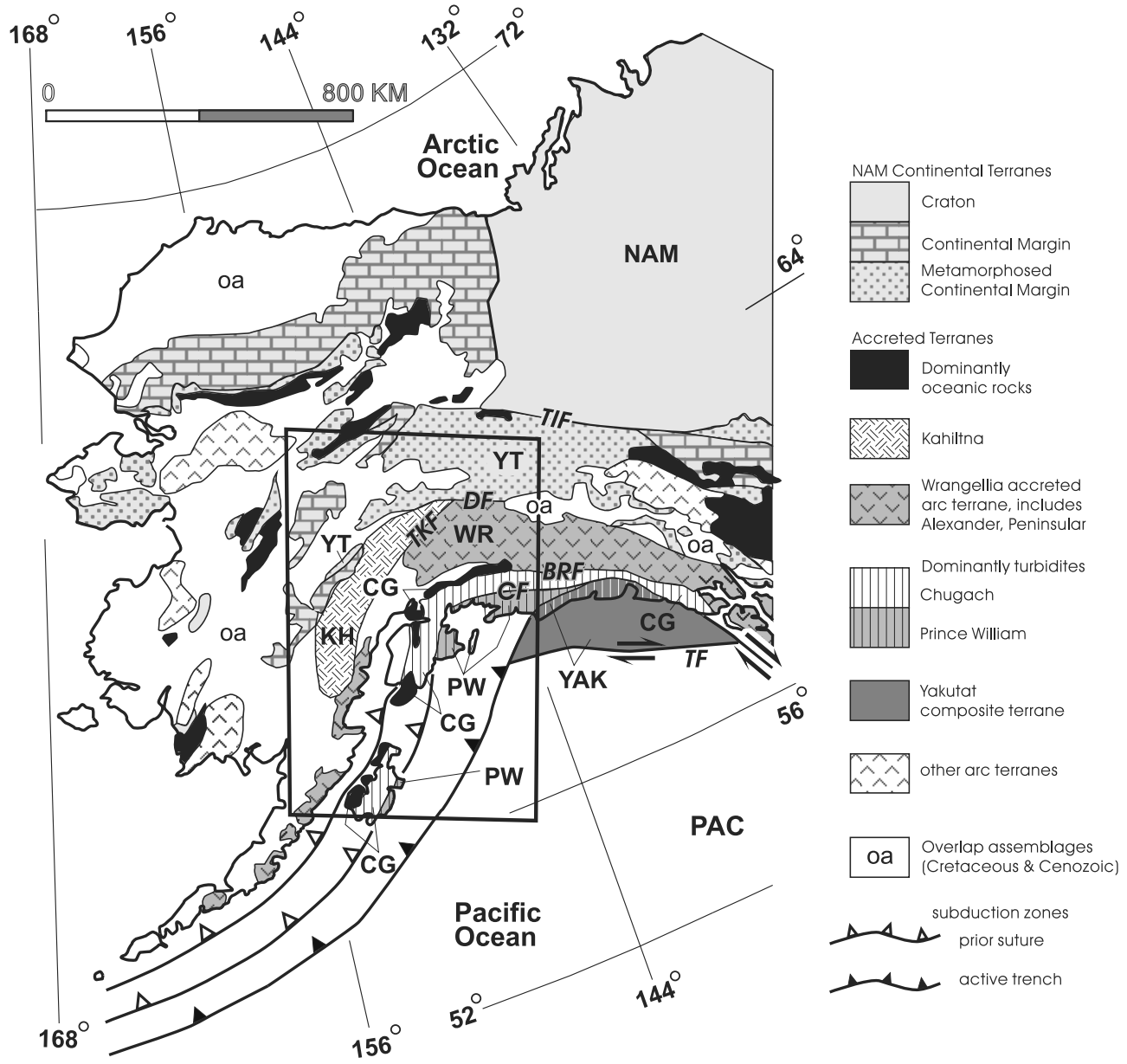

Figure 1. Tectonic setting of Alaska. Generalized terrane map by *Nokleberg et al.* [2000]. Rectangle shows grid area for velocity inversion. Faults are TIF, Tintina; DF, Denali; TKF, Talkeetna; BRF, Border Ranges; CF, Contact; TF, Transition. Terranes are YT, Yukon-Tanana; KH, Kahiltna; WR, Wrangellia composite; CG, Chugach; PW, Prince William; YAK, Yakutat.

aperture of the Alaska regional seismic network coupled with the high level of seismic activity provides a unique opportunity for three-dimensional studies. Our goal is to obtain the 3-D image that is defined by the data, without specifying a prescribed model. To this end, we incorporate the extensive active source data directly into the velocity inversion, and we start with a 1-D model without specified layer boundaries.

2. Previous Work

[5] Over the past 25 years, a number of investigations of the seismicity and tectonics of the southern and central Alaska have been carried out. Early studies concentrated on attempts to use earthquake locations to delineate geometry of the subducting plate [*van Wormer et al.*, 1974; *Stephens et al.*, 1984; *Pulpan and Frohlich*, 1985; *Page et al.*, 1989]. Later seismicity studies worked on improving earthquake locations and providing better seismological constraints on tectonics of the region [*Estabrook et al.*, 1992; *Doser et al.*, 1997; *Ratchkovski et al.*, 1997, 1998; *Doser et al.*, 1999; *Doser and Lomas*, 2000; *Doser and Brown*, 2001; *Ratchkovski and Hansen*, 2002]. A few tomographic studies used regional seismic data to constrain the extent and properties of the subducting plate [*Kisslinger and Lahr*, 1991; *Zhao et al.*, 1995; *Searcy*, 1996] and upper plate crust [*McNamara and Pasyanos*, 2002]. These tomographic studies inferred the subducting Pacific plate to be 45–55 km

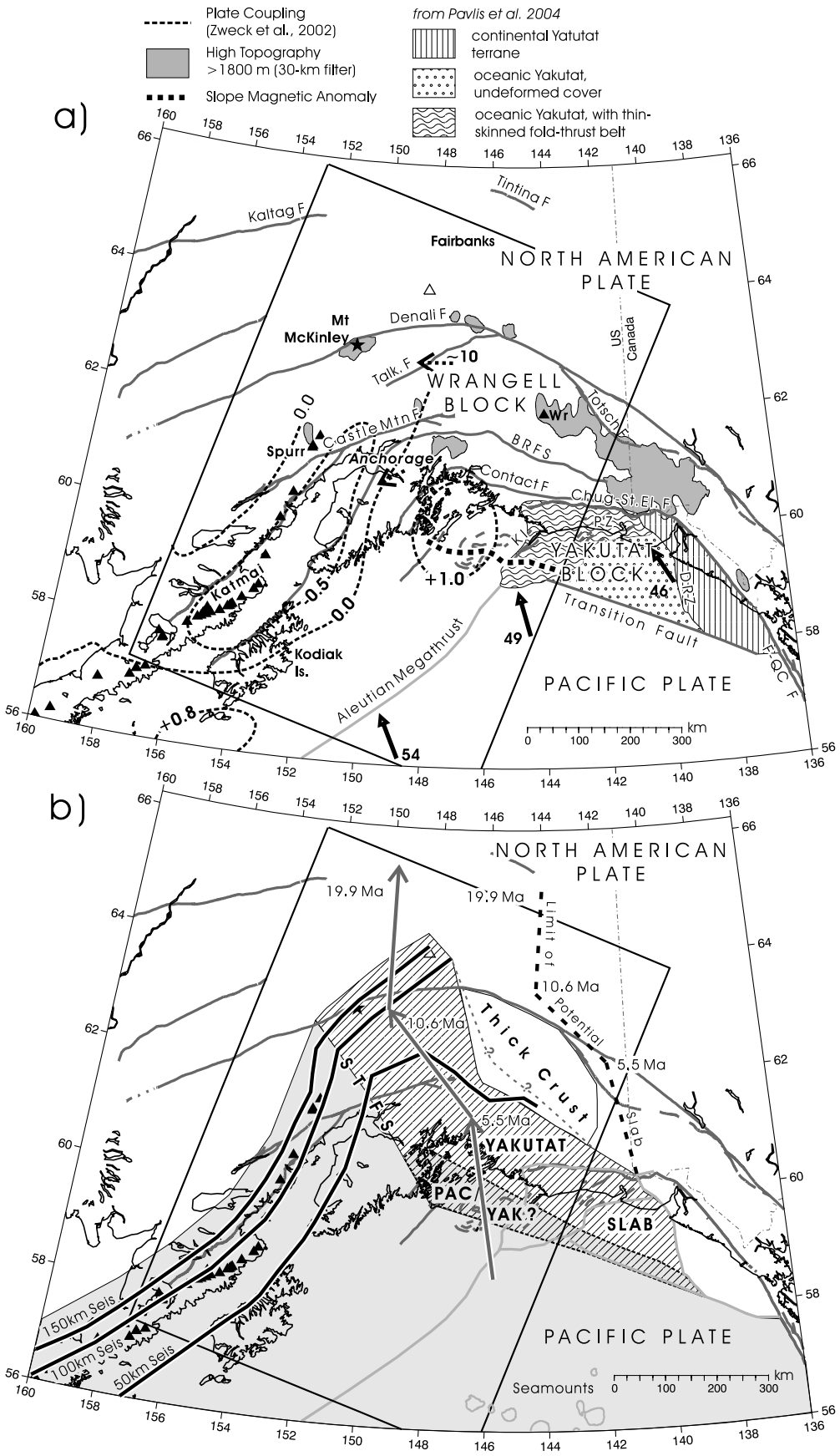
a)
Plate Coupling
(Zweck et al., 2002)
High Topography
>1800 m (30-km filter)
Slope Magnetic Anomaly
from Pavlis et al. 2004
continental Yatutat terrane
oceanic Yakutat, undeformed cover
oceanic Yakutat, with thin-skinned fold-thrust belt
Tintina F
Kaltag F
Fairbanks
NORTH AMERICAN PLATE
Mt McKinley
Denali F
US
Canada
Talk. F
10
WRANGELL BLOCK
Wr
Totschunda
0.0
Castle Mtn F
Spurr
Anchorage
BRFS
Contact F
Chugach-St. Elias F
PWS
YAKUTAT BLOCK
Katmai
-0.5
-0.0
+1.0
46
Transition Fault
49
Kodiak Is.
Aleutian Megathrust
PACIFIC PLATE
EQC F
+0.8
54
km
0 100 200 300
b)
NORTH AMERICAN PLATE
19.9 Ma
19.9 Ma
Limit of Potential Thick Crust
10.6 Ma
10.6 Ma
5.5 Ma
STFS
5.5 Ma
YAKUTAT
PAC
YAK ?
SLAB
slab
150km Seis
100km Seis
50km Seis
PACIFIC PLATE
Seamounts
km
0 100 200 300

Figure 2

thick with a *P* wave velocity 3–6% higher than that of the surrounding mantle, presumably because it is cold. However, the top of the plate shows much structure. High-frequency guided waves at > 100 km depth beneath Cook Inlet, show a 2- to 6-km-thick low-velocity layer, 5–8% slower than surrounding mantle, inferred to represent oceanic crust not yet metamorphosed to eclogite [*Abers and Sarker*, 1996; *Abers*, 2005].

[6] From the mid-1980s to early 1990s, the U.S. Geological Survey and collaborators acquired geological and geophysical data along the Trans Alaska oil pipeline extending from Valdez to Prudhoe Bay [*Stone et al.*, 1986]. As part of this transect, the Trans-Alaska Crustal Transect (TACT), several controlled source studies, including both deep crustal reflection and refraction profiles, provide a detailed and continuous velocity and structural model for the crust along the transect. Transect results from onshore were presented in numerous individual publications [*Fisher et al.*, 1983, 1989, 2004; *Brocher et al.*, 1989, 1991, 1994, 2003, 2004; *Brocher and Moses*, 1990, 1993; *Flueh et al.*, 1989; *Goodwin et al.*, 1989; *Fuis and Plafker*, 1991; *Fuis et al.*, 1991, 1997; *Wolf et al.*, 1991; *Beaudoin et al.*, 1992; *Beaudoin*, 1994; *Levander et al.*, 1994]. The crustal structure of the southern continental margin in Prince William Sound by TACT and in the Cook Inlet by EDGE was studied using marine air guns, marine reflection profiling, and ocean bottom and land-based recorders [*Moore et al.*, 1991; *Brocher et al.*, 1994; *Ye et al.*, 1997].

[7] A new data set has shown that the tectonic processes inferred near surface can be followed into the lower mantle. In 1999–2001, the Broadband Experiment Across the Alaska Range (BEAAR) sampled at high density the broadband wavefield beneath the Alaska Range. In this data set, the upper 15–20 km of the downgoing plate consists of a low-velocity layer, prominent on receiver functions to depths of 120 km, which had been interpreted by *Ferris et al.* [2003] to be subducted thickened crust, likely the Yakutat terrane, which is presently colliding with the trench. Subduction of this buoyant lithosphere was speculated to drive the shallowing of the slab and mountain building in the Alaska Interior, one of the first compelling observations of subduction of thick crust. Observations made in the present paper greatly expand on our understanding of this feature, and its relationship to Alaska tectonics. In a complementary study, *Veenstra et al.* [2006] has shown, via receiver function inversion, that the upper plate crust varies in thickness only partly in compensation of topographic loads and that terrane boundaries correspond to important changes in the mechanism or horizon of compensation.

[8] Several BEAAR results also highlight the structure of the mantle wedge beneath central Alaska. *Stachnik et al.* [2004] show that the wedge is highly attenuating (low *Q*) where the slab is more than 80 km deep and therefore hot, and they find the shallower mantle wedge has high *Q*, indicating cold temperatures. With receiver function multiples, *Rossi et al.* [2006] showed that the upper mantle wedge beneath the Alaska Range exhibits unusually low Poisson's ratio <0.25. *Abers et al.* [2006] developed thermal models that use realistic mantle rheology.

3. Tectonic Setting

[9] Alaska has developed where the northwestern part of the North American (NAM) continental margin has overridden various subducting plates since Jurassic time, including Kula/Resurrection, Pacific, and Pacific plus Yakutat (Figure 1). The tectonic syntheses by *Plafker and Berg* [1994] and *Nokleberg et al.* [2000] are summarized here. The Denali fault forms the southern boundary of the NAM continental terranes (Figures 1 and 2). North of the Denali fault, deformation of the NAM continental margin created continental margin terranes such as the Yukon-Tanana terrane, which was displaced 450 km along the Tintina strike-slip fault inboard of the subduction zone. South of the Denali fault, the subducting slabs transported oceanic and arc terranes from great distances, and accreted them to the margin of NAM.

[10] The Wrangellia composite terrane has variably metamorphosed magmatic arc and oceanic plateau material that was transported northward about 20° by Late Jurassic time. The Kahiltna terrane overlies the western part of the Wrangellia terrane, and it is separated from the Yukon-Tanana terrane by the Denali fault. The Kahiltna flysch was tectonically thickened and underthrust during mid-Cretaceous to Eocene time [e.g., *Ridgway et al.*, 2002]. The collapse of the basin in which it was deposited is thought to have occurred by northward subduction, and

Figure 2. (a) Crustal tectonics, after *Haeussler et al.* [2000] and *Pavlis et al.* [2004]. Dashed arrows show hypothesized direction of motion of the Wrangell block with respect to NAM. Solid arrows show plate motion (mm/yr) for Pacific-NAM [*DeMets et al.*, 1994] and Yakutat-NAM [*Fletcher and Freymueller*, 1999]. Plate coupling shown with dashed black lines is from geodesy [*Zweck et al.*, 2002]: 1.0, fully coupled; +0.8, high coupling; 0.0, no coupling; −0.5, negative coupling or trenchward motion. High topography is shown by 1800-m contour of 30-km median-filtered topography. Star, Mount McKinley; solid triangles, active volcanoes; open triangle, Buzzard Creek Maar. BRFS, Border Ranges Fault System; KI, Kayak Island; PZ, Pamplona Zone; DRZ, Dangerous River Zone. (b) Subducting plate as inferred by this study. Gray, Pacific; striped, Yakutat; overlap, schematic region of Pacific underthrust Yakutat (actual amount not certain). Thick crust east of the slab is in the overlying plate. Bold lines show slab depth as defined by seismicity. STFS, Subducted Transition Fault System. Seamounts are from bathymetry. Gray arrows show cumulative plate motions for the last 20 Myr for a spot on the Pacific plate with respect to NAM (e.g., the point labeled 19.9 Ma would have been at the initial point on the outboard of the trench 19.9 Ma). For the end-member hypothetical case of zero Pacific-Yakutat displacement and a dipping slab, the dashed line (labeled limit of potential slab) shows cumulative motion for a point of the oceanic Yakutat terrane and thus limits the potential "missing" Yakutat slab. The plate motions are from *Stock and Molnar* [1988].

collision of Wrangellia [e.g., *Plafker et al.*, 1994a]. The Border Ranges fault system forms the southern margin of Wrangellia, and it is the backstop fault for several successive accretionary wedge terranes. The Chugach terrane is the earliest part of the accretionary complex and consists of mélange of oceanic rocks, deep marine turbidites, and younger granitic plutons. The Prince William terrane is dominantly turbidites, blocks of oceanic volcanic rocks, and younger granitic plutons, and was sutured to the Chugach terrane along the Contact fault.

[11] The Yakutat is the most recently accreted terrane, outboard of the Prince William terrane (Figure 1). The Yakutat terrane has two parts: on its east side are Cretaceous accretionary complex rocks similar to the Chugach or Prince William terranes; on its west side are Eocene volcanic rocks with oceanic affinities [*Plafker*, 1987]. These two parts of the terrane are thought by *Plafker et al.* [1994a] to have been brought together by transform margin faulting. Both parts of the Yakutat terrane are covered by late Miocene to Plio-Pleistocene age marine to nonmarine sedimentary rocks. The Transition fault bounds the southwestern margin of the terrane, and it is most likely an active suture between the Yakutat and Pacific plates [*Fletcher and Freymueller*, 1999, 2003].

[12] The current active crustal tectonics are summarized in Figure 2a. The primary feature is the subduction of the Pacific plate along the Aleutian subduction zone, which extends several thousand kilometers to the west of Kayak Island. This results in great thrust earthquakes, where the shallow subducted plate is coupled to the overlying plate and there is extensive arc volcanism farther inboard. The plate coupling varies along strike with some patches where it is very strong ($\geq$1.0) and others where it is very weak ($\approx$0.0), and inboard it becomes negative or trenchward [*Zweck et al.*, 2002]. The Yakutat terrane has been inferred to be essentially attached to the Pacific plate [*Bruns*, 1983; *Brocher et al.*, 1994] or to be deforming as a distinct microplate [*Pavlis et al.*, 2004, and references therein].

[13] The plate boundary deformation zone extends from the trench to the Denali fault system, and perhaps even to the North Slope [*Plafker et al.*, 1994b]. The Denali fault has about 10 mm/yr right-lateral slip [*Matmon et al.*, 2004]. The geodetic data from the Yakutat microplate indicate about 45.6 mm/yr northwest motion parallel to the Fairweather Fault [*Fletcher and Freymueller*, 2003]. Thus much of the Yakutat collision is accommodated as thrust faulting in the region south of the Denali Fault system, including extreme uplift of the Alaska coast ranges and the St. Elias orogen. The southeastern active strand of the Denali Fault system is the Totschunda Fault, which projects toward and may, in the subsurface, connect with the Queen Charlotte–Fairweather Fault system [*Richter and Matson*, 1971]. South of the Denali Fault the region has been referred to as the Wrangell crustal block [*Lahr and Plafker*, 1980], which is being extruded to the west [*Haeussler et al.*, 2000], with most shear along the Denali Fault system. This Wrangell block is also internally deforming as indicated by the Castle Mountain Fault, which is an active right-lateral strike-slip fault within the broad deformation zone. Mount McKinley is the highest peak in the Alaska Range and is actively uplifting at 1 mm/yr [*Fitzgerald et al.*, 1995].

[14] The relationship between the subducting slab and arc volcanism is variable (Figure 2b). Southwest of Mount Spurr, the chain of arc volcanoes lie above the 100-km isobath of the subducted slab. North and east of Mount Spurr, however, there is essentially no active volcanism until the longitude of the Wrangell volcanoes, although the subducted slab extends 300 km northeast of Mount Spurr, as indicated by the slab seismicity (contoured in Figure 2b). Quaternary volcanic rocks have been found only at the Buzzard Creek Maars, a small, 3000-year-old basaltic-andesite vent at the easternmost edge of the intermediate-depth seismic zone [*Nye*, 1999] (open triangle Figure 2b). The Wrangell volcanoes constitute a separate volcanic field to the north of the Yakutat terrane (Figure 2). Volcanism has occurred in the Wrangell volcanic field over the last $\sim$30 Myr, but it appears to have dramatically decreased in the last 500,000 years [*Richter et al.*, 1990].

[15] In this paper, we compute images of the subducted oceanic Yakutat terrane beneath central Alaska. According to *Plafker* [1987], the Yakutat terrane has subducted with the Pacific plate for up to 600–1000 km north of the Aleutian trench, and *Ferris et al.* [2003] show that it persists in the mantle to 140 km depth, at least 500 km north of the trench. The plan view shape of the Yakutat slab from our results is summarized in Figure 2b so that the reader can compare it to the 3-D velocity plots which follow. The arrows in Figure 2b show how a point on the Pacific slab might have subducted over the past 19.9 Myr.

4. Data

[16] First installations of the Alaska regional seismic network date back to the late 1960s to early 1970s. The current network configuration contains about 300 sites, the majority of which are equipped with short-period vertical sensors. The largest station concentration is in southern and central Alaska where the post-1990 earthquake catalog is complete to about magnitude 1.4 [*Wiemer and Wyss*, 2000]. Starting in 1998, a number of seismic stations were upgraded with modern digital broadband seismometers in addition to the installation of many new broadband sites. Currently, the combined network includes over 40 broadband sites. The network is operated jointly by the Alaska Earthquake Information Center (AEIC), Alaska Volcano Observatory (AVO) and the West Coast and Alaska Tsunami Warning Center (WCATWC). All data are collected at the Alaska Earthquake Information Center in Fairbanks, where the earthquake data are processed and archived. The AEIC hypocenter determination procedures changed in 1998, which could bias tomography where such hypocenters are held fixed. However, our method of simultaneous inversion for hypocenters and 3-D velocity avoids this problem. In addition to the regional seismic network, a vast data set was collected during the BEAAR PASSCAL experiment conducted in 1999–2000 across the Alaska Range in central Alaska [*Veenstra et al.*, 2006; *Stachnik et al.*, 2004] (Figure 3a). At its peak, 36 broadband sites were in simultaneous operation. In November 2002, in the wake of the Denali Fault earthquake, a temporary network of 26 broadband and strong motion instruments were installed to monitor the aftershock activity [*Ratchkovski et al.*, 2003].

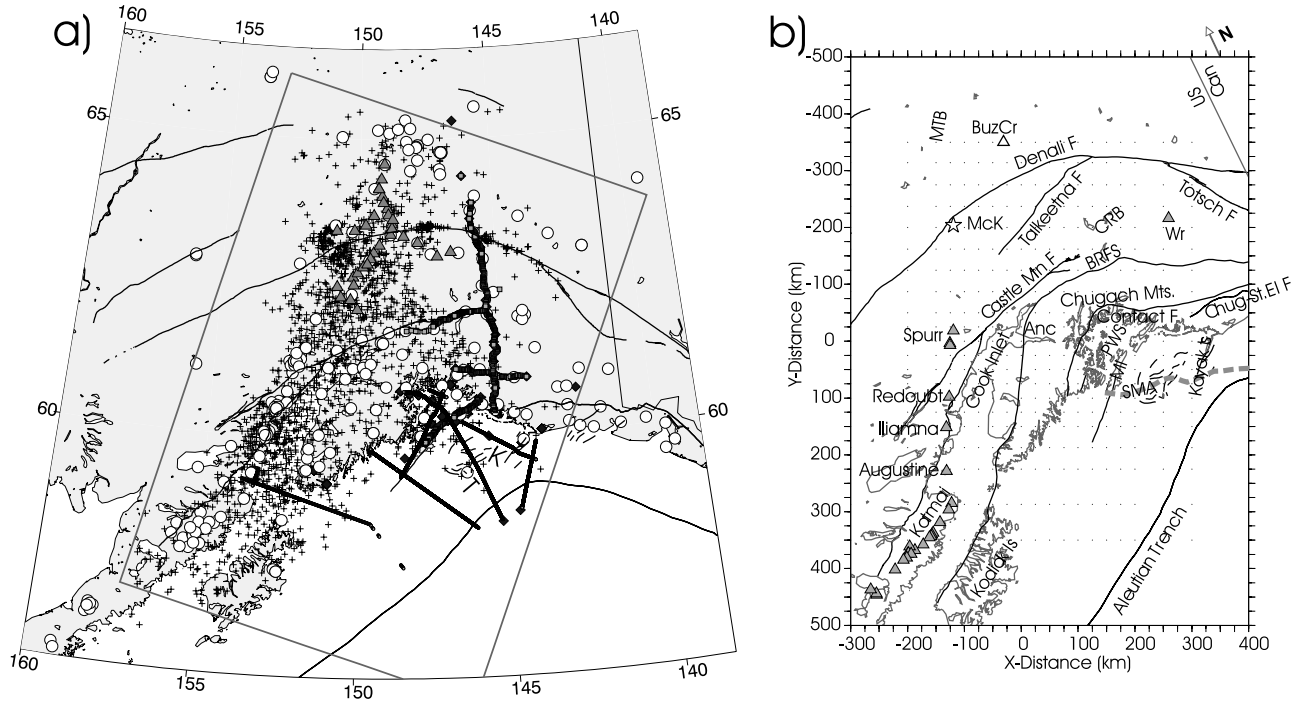

Figure 3. (a) Stations and sources. Rectangle shows grid area for velocity inversion. Plus, inversion earthquakes; diamond, shots. Stations are circle, AEIC; triangle, BEAAR; small square, TACT land; small circle, offshore air gun. T (TACT) and K (Kayak) offshore profiles are shown in Figure 13. (b) Grid for velocity inversion, with labeled features, for comparison to Figures 4–7, where annotation would distract from images. Basins are CRB, Copper River; MTB, Middle Tanana. Triangles are volcanoes as labeled Wr, Wrangell; BuzCr, Buzzard Creek Maar. Faults are labeled; BRFS, Border Ranges Fault System. SMA, slope magnetic anomaly; PWS, Prince William Sound; MI, Montague Island.

This network was in operation for seven months, and it is also used in our study.

[17] The best tomographic image will be obtained from evenly distributed ray paths, and hence we selected the most appropriate data set based on spatial distribution and data quality, rather than simply taking a temporal subset. There is abundant seismicity recorded by AEIC. The data set contained 1752 earthquakes, with 64,317 *P* arrivals and 19,937 *S-P* arrivals. Events from 1991–2003 were used, with most from 1997 and later when the network was improved. Location quality was inferred from the number of observations, azimuthal gap, and ratio of depth to distance to nearest station (RZD). Most selected events were very well constrained with 30–70 observations, gap < 120°, and RZD < 2, but weaker events were included that improve spatial distribution. Most events had magnitudes of 2.5–4.0, and 364 events had magnitude >4.0. During the BEAAR time period, 200 distributed events with magnitude ≥2.0 were selected. The majority of the AEIC's *S* arrivals are from vertical component stations and the *S* data may include some misidentified picks. Limiting the data set to selected, well-constrained hypocenters means that occasional bogus *S* picks will not affect the hypocenters, but they will have high residuals and be greatly downweighted in the inversion.

[18] Controlled source data supplement the earthquake data (Figure 3a). The TACT land profiles in southern Alaska were reported and summarized by *Fuis et al.* [1991]. We used their first arrival data and also timed arrivals on additional TACT shots north of the Denali fault [*Beaudoin et al.*, 1992; *Brocher et al.*, 2004], giving 2836 *P* arrivals. The TACT 1988 and EDGE 1989 onshore-offshore data constituted onshore recordings of air gun shots [*Brocher et al.*, 1994; *Brocher and Moses*, 1993], and 11,798 first arrivals were incorporated as "shots" at the onshore recording sites with "stations" at the air gun locations. Bathymetry corrections are included, and station delays are allowed for the air gun stations to help account for near-surface sediments.

5. Method

[19] Arrival times of local earthquakes and shots were used in a simultaneous inversion for hypocenters, three-dimensional (3-D) *P* velocity, and V_p/V_s ratio [see *Thurber*, 1983, 1993; *Eberhart-Phillips*, 1990, 1993; *Eberhart-Phillips and Michael*, 1998]. V_p/V_s is an important parameter in characterizing rock properties and rheology [e.g., *Christensen*, 1996]. Directly obtaining V_p and V_p/V_s, rather than V_p and V_s, makes it feasible to interpret V_p/V_s heterogeneity, including resolution. We have many more *P* arrivals than *S* arrivals. Solving for V_p/V_s makes the assumption that given a 3-D heterogeneous V_p model and unknown V_s, it would be most reasonable to estimate a V_s model from the V_p using a constant V_p/V_s than to assume a homogeneous 1-D V_s model.

[20] Seismic methods measure material properties along the seismic propagation path from the source to the receiver.

Table 1. The 1-D Velocity Model

Depth (0 = SL), km	V_p, km/s
−1.0	2.90
2.0	5.10
6.0	6.05
15.0	6.35
24.0	6.60
33.0	7.15
48.0	7.87
65.0	8.12
85.0	8.20
110.0	8.24
140.0	8.30
190.0	8.44
350.0	8.84

The source locations are unknowns in inverting earthquake data. Thus consideration must be given during the inversion procedure to obtaining a reasonable velocity model from the nonuniform sampling of the 3-D volume. We desire a crustal model that is useful for other applications, such as defining 3-D rheology in numerical deformation models, so we aim for a reasonable model even in areas where we have little seismic resolution. This guides our strategy of gradational inversions and linked nodes.

[21] The velocity of the medium is parameterized by assigning velocity values at the intersections (nodes) of a 3-D grid (Figure 3b). The ray paths are calculated with an approximate 3-D ray-tracing algorithm that produces curved nonplanar ray paths which are defined by points more finely spaced than the velocity nodes. This is a Cartesian grid with conversions done using Alaska state plane coordinates and an earth-flattening transformation [*Buland and Chapman*, 1983] for velocity during ray tracing. Only observations with epicentral distances less than 300 km are included, and distances from 75 to 300 km are downweighted. The solution is obtained by iterative, damped least squares. Damping leads to a conservative solution that fits the data well with few artifacts. Thus selected damping parameters greatly reduce data variance with moderate increases in model variance [*Eberhart-Phillips*, 1986]. For each iteration, new ray paths are determined, the hypocenter solution is included, and parameter separation is carried out. The full resolution matrix is also calculated. Throughout the inversion, weighting is applied to each observation, based on observation quality, source-receiver distance, and size of the residual, so that residuals greater than 1.50 s are greatly downweighted. When the model velocities are not close to the actual velocities, high residuals may be more representative of velocity heterogeneity, and thus in initial inversions, high downweighting was conservatively limited to residuals greater than 6.00 s.

[22] We performed a series of inversions of increasing complexity: 1-D, coarse 3-D and fine 3-D. Such a series of progressive inversions will have a smooth regional model in places of low resolution. The 1-D initial velocity model (Table 1) and initial hypocenters were obtained through simultaneous inversion of the earthquake data for 1-D V_p, station corrections and hypocenters, with the AEIC south central 1-D model as the starting model. Offshore, the initial model had a 3-D model for the Pacific plate, because the 1-D earthquake model is not representative and might result in artifacts [*Eberhart-Phillips and Bannister*, 2002]. The V_p/V_s model is initially 1.75, which is the best fitting uniform V_p/V_s.

[23] The coordinates of the velocity grid were chosen to parallel the deep slab seismicity in the region (Figure 3). The y axis is positive to the southwest and the x axis is positive to the southeast. The z grids were chosen at −1, 2, 6, 15, 24, 33, 48, 65, 85, 110, 140, and 190 km depths. The coarse 3-D inversion had x and y grids with 50–125 km spacing, and the fine 3-D inversion had spacing halved with grids spaced 25–63 km. The fine 3-D model achieved a 70% reduction in traveltime data variance from the 1-D model. This included a larger solution norm for V_p than for V_p/V_s and greater variance reduction for P traveltime (81%) than for S-P traveltime (58%). The S times are harder to pick accurately and so include more noise that is not fit by the 3-D inversion.

[24] Resolution is shown in Figures 4 and 5. The resolution matrix describes the distribution of information for each node, such that each row is the averaging vector for a parameter. The relative size and pattern of the off-diagonal elements show the way the information is smeared. For a node to be adequately resolved, its resolution should be peaked and should have no significant contribution from nodes that are not adjacent. For a succinct way of assessing the resolution, we calculate the spread function (SF) [*Michelini and McEvilly*, 1991], which describes how strong and peaked the resolution is for each node. For low values of SF, <2.5, the resolution is good and the model V_p or V_p/V_s is representative of the volume surrounding the given node. For SF of 2.5–3.5, the nodes show meaningful velocity patterns, but they may incorporate smearing and the size of velocity perturbations may be relatively small. Nodes with SF > 4.25 are masked in the velocity plots. We also illustrate the pattern of image blurring in low-resolution areas by showing contours of the averaging vectors for nodes that have significant smearing. From each row of the resolution matrix we compute smearing contours where the resolution is 70% of the diagonal element [*Reyners et al.*, 1999]. Resolution contours are shown only for those nodes which have smearing such that the resolution contour extends beyond an adjacent node. At other nodes, we would expect the spatial averaging to be represented by the grid spacing.

[25] The pattern of V_p/V_s resolution is similar to V_p, but there is overall less information because of fewer observations. V_p/V_s resolution is low offshore and weaker along the TACT land profile where controlled source data are incorporated into the 3-D V_p model, but do not provide S arrivals.

6. Results

6.1. Hypocenters

[26] The 3-D hypocenters show improved locations based on residuals, and also on seismicity patterns. The hypocenters do not differ in a systematic manner from the 1-D hypocenters. The locations generally differ by less than 6 km horizontally and vertically with 10% changing more than 10 km in depth from the 1-D hypocenters. The 3-D seismicity in the subducted slab forms a narrow zone bending smoothly, and appears more appropriate than the 1-D hypocenters for interpreting subduction features. The

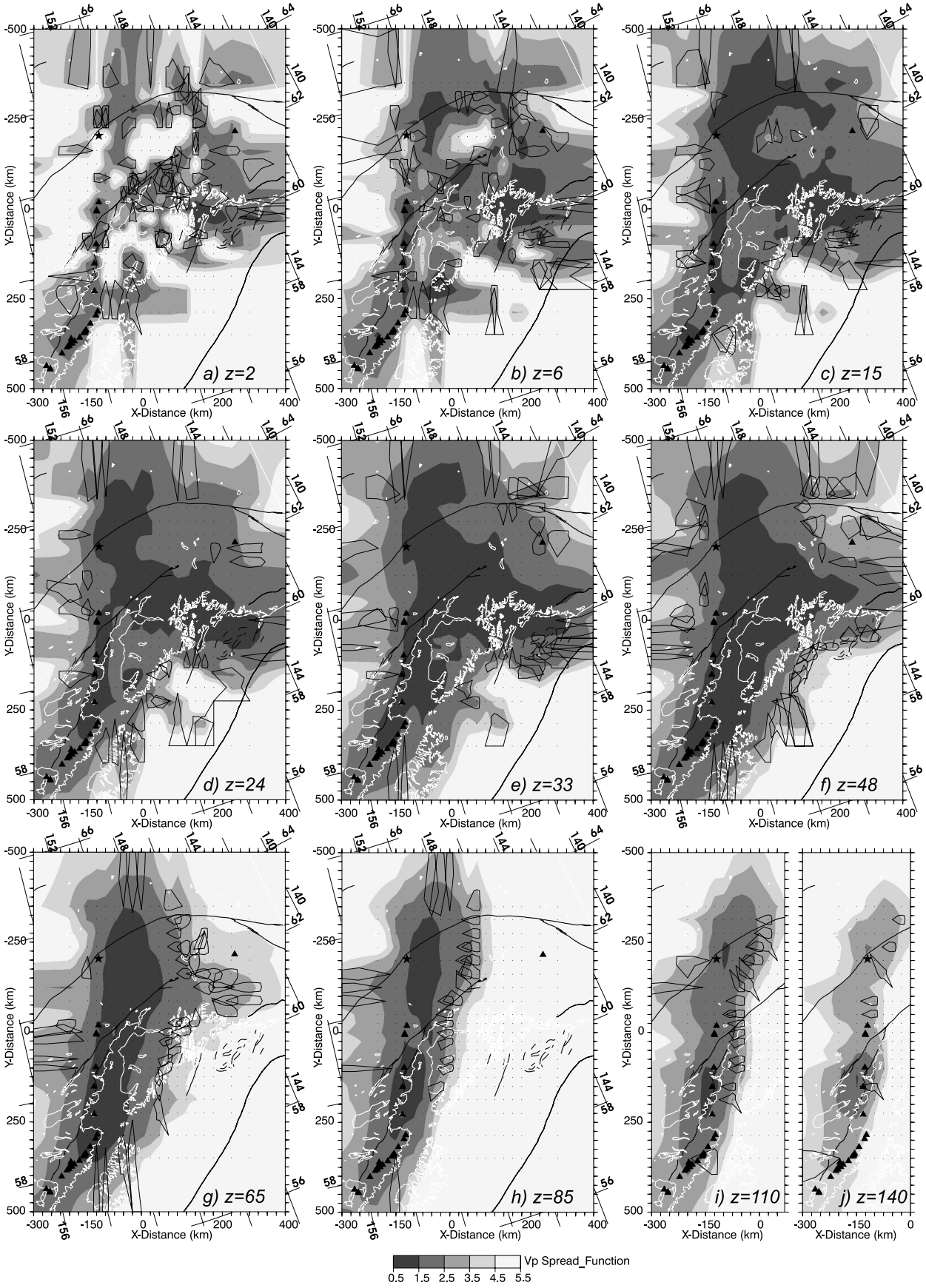

Figure 4. Map views of resolution for V_p, showing spread function (SF) and 70% smearing contours for nodes that have significant smearing. Darker gray (SF < 2.5) is good resolution. Z equals depth of image in kilometers. Resolution area decreases with depth so Figures 4i and 4j do not cover the whole area.

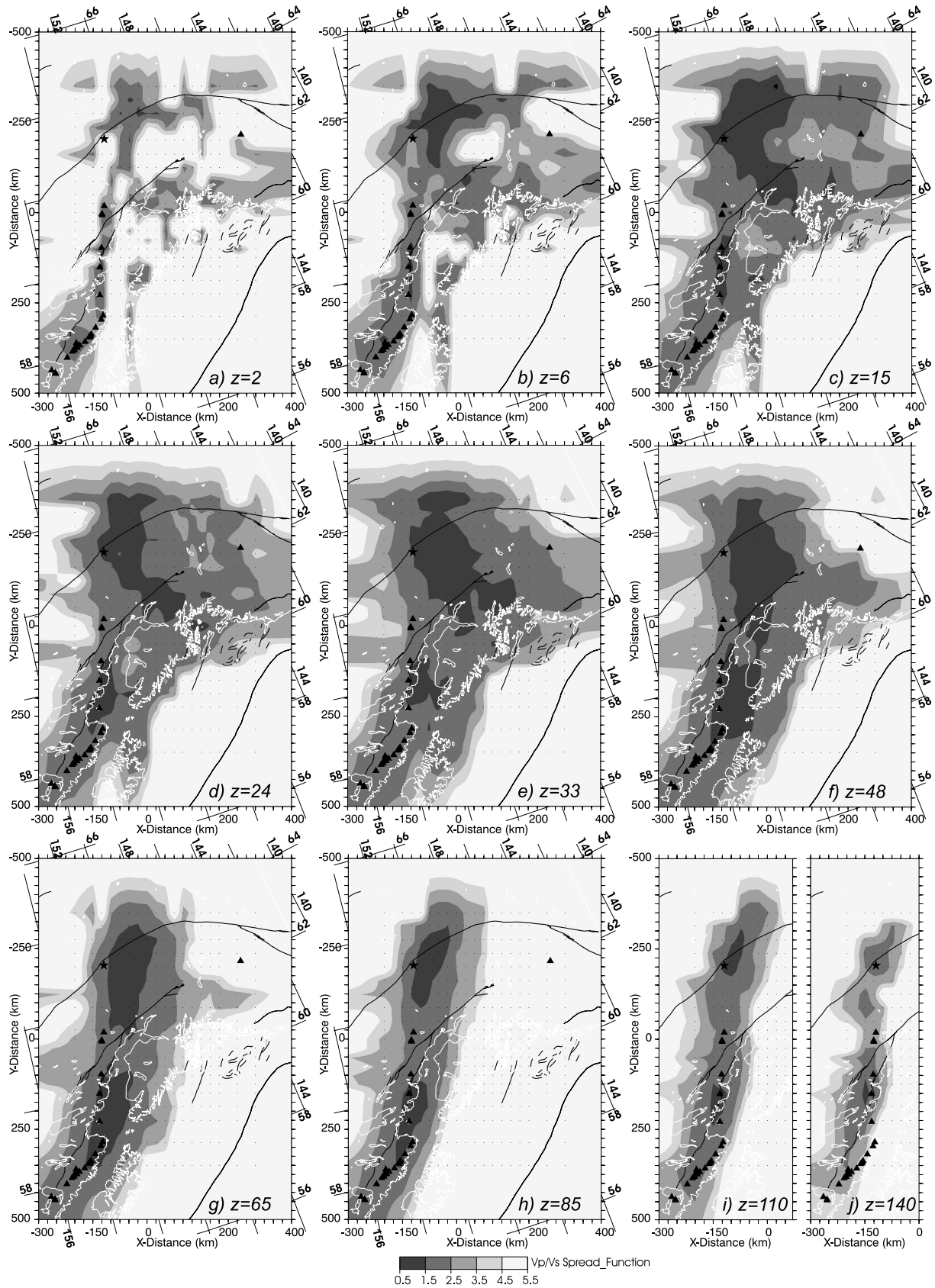

Figure 5. Map views of resolution for V_p/V_s, showing spread function (SF) and 70% smearing contours for nodes that have significant smearing. Darker gray (SF < 2.5) is good resolution. Z equals depth of image in kilometers. Resolution area decreases with depth so Figures 5i and 5j do not cover the whole area.

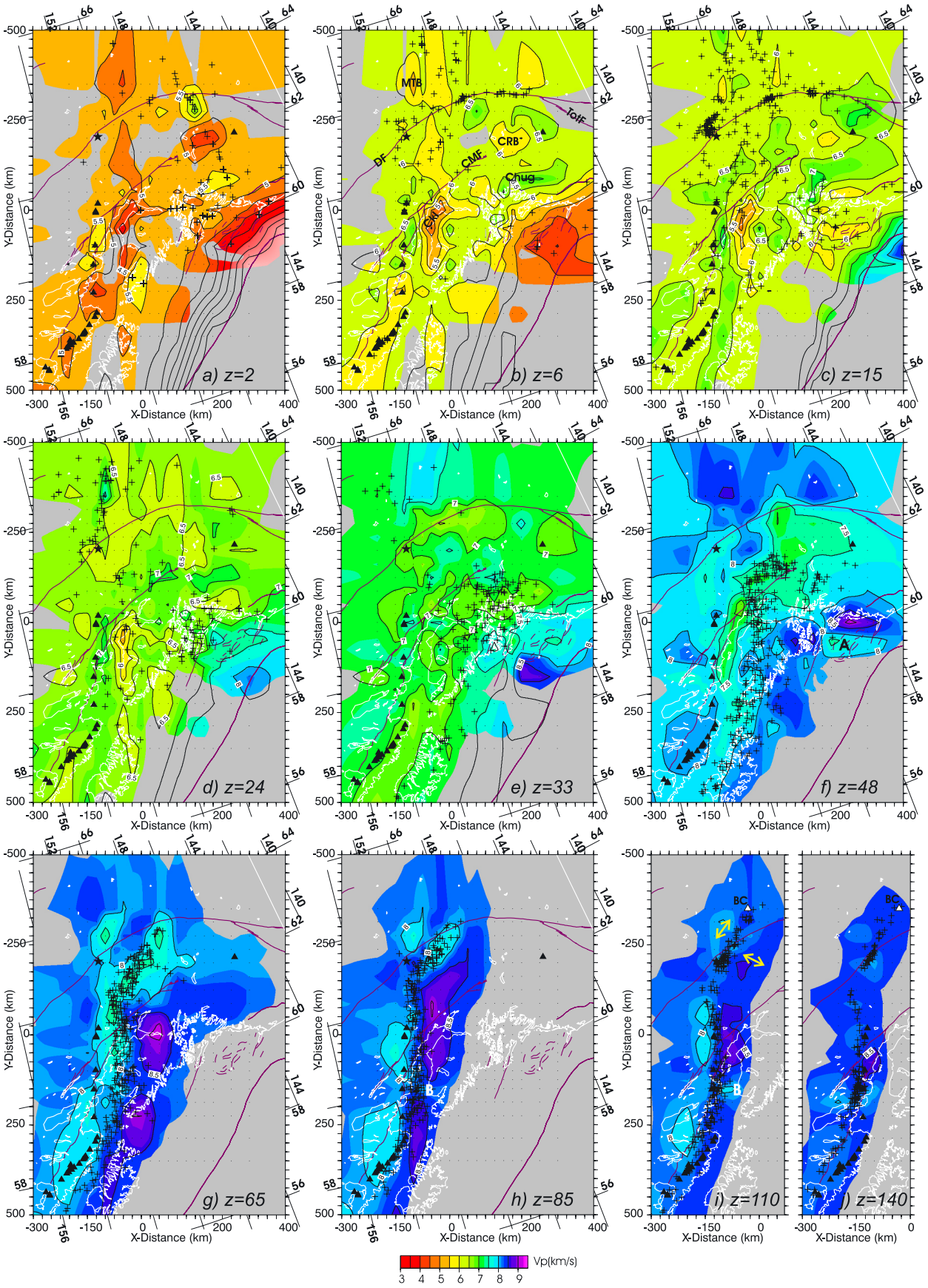
a) z=2
b) z=6
c) z=15
d) z=24
e) z=33
f) z=48
g) z=65
h) z=85
i) z=110
j) z=140
MTB
DF
CMF
CRB
Chug
ToIF
A
B
BC
X-Distance (km)
Y-Distance (km)
Vp(km/s)
3 4 5 6 7 8 9

Figure 6

standard errors average 0.26 km horizontal and 0.47 km vertical, and the average RMS residual is 0.14 s. This study only uses a subset of the recorded data, but illustrates the potential for more comprehensive relocations of deep seismicity with the 3-D velocity model.

6.2. Upper Crust

[27] Velocity variations in the upper crust (2–15 km depth, Figures 6a–6c and 7a–7c) primarily reflect, on the low-velocity end, thick Cenozoic sedimentary basins and, on the high-velocity end, mafic crustal blocks. The spatial resolution at these shallow depths is strongly affected by the station and source distribution and so it is quite patchy, especially for the V_p/V_s model (Figures 4a–4c and 5a–5c). The model resolution is best near the center of the model, where the station and source densities are highest. The model resolution is poorest near the Totschunda and eastern Denali faults and along the western periphery of the grid. Thus the full geographic extent of some of the velocity features identified in the models is not clear.

[28] The V_p model in the upper crust reflects low-velocity anomalies colocated with a series of thick Cenozoic sedimentary basins. Controlled source studies along the TACT corridor found that as a rule of thumb, sedimentary rocks filling these basins have compressional wave velocities less than 4.5 km/s [*Fuis et al.*, 1991; *Brocher et al.*, 2004]. Velocities less than 4.5 km/s are not generally observed at depths of 6 km or more, suggesting that none of these basins approach this thickness, or that compaction increases velocities at these depths.

[29] The most prominent basin is the Cook Inlet forearc basin, with up to 5 km of Tertiary sedimentary deposits [*Kirschner and Lyon*, 1973]. Cook Inlet is underlain by a low-velocity anomaly to 24-km depth (CkI, Figure 8a), having a compressional wave velocity of 5.2 km/s at 15-km depth. We expect some vertical smearing of the low velocities in the basin, because the inlet lacks hypocenters less than 15 km deep. The inlet is not distinctive in the V_p/V_s solution, although it has slightly high V_p/V_s of 1.78 where there is resolution, consistent with overpressured zones inferred by *Bruhn et al.* [2000]. The laterally extensive, 5-km-thick Copper River Basin [*Nokleberg et al.*, 1989; *Fuis et al.*, 1991] is associated with a broad region of low *P* wave velocity, 5.5 km/s at 6-km depth, that is 75 km wide at 15 km depth (CRB, Figures 6a–6c). It has moderate V_p/V_s of 1.75. The Middle Tanana Basin is associated with similarly low compressional wave velocity, 5.5 km/s, at 6-km depth (MTB, Figures 6a and 6b).

[30] The most prominent high-velocity anomaly in the upper crust is located in the Chugach Mountains, where the model yields a *P* wave velocity of 6.75 km/s at 6-km depth and 7.0 km/s at 15-km depth (Figures 6b and 6c). This high-velocity anomaly loses prominence below this depth, as it is underlain by a velocity reversal, to $V_p < 6.5$ km/s. The southern edge of the high-velocity anomaly is defined by a sharp velocity gradient that may represent the Contact fault system (Figures 9a and 9b). Our model is relatively coarse and does not specify faults, but it is consistent with a north dipping fault system, as previously mapped by *Bol and Gibbons* [1992] in central and western Prince William Sound. The Chugach Mountains are underlain by a series of gently north dipping intermediate to ultramafic layers, which are slivers of oceanic crust and mantle, thought by *Fuis et al.* [1991] to be subcreted remnants of the former Kula plate. The generally high velocities of the Chugach Mountains originate from these accreted oceanic layers. South of the Totschunda fault, there is an upper crustal high-velocity anomaly having V_p of 6.8 km/s at 15 km depth (Figure 6c), corresponding to a region with extensive mafic plutons [*Miller and Richter*, 1994]. The East Glenn Highway TACT line ran through the northwest corner of this anomaly, and it provides evidence for localized high-velocity anomalies of 6.6 km/s which were interpreted as a diorite body [*Goodwin et al.*, 1989].

[31] Another high-velocity anomaly is imaged between 15- and 24-km depths in the vicinity of the Cook Inlet volcanoes (Figures 6c and 6d), which is also a region of extensive Late Cretaceous–early Tertiary plutonism [*Reed and Lanphere*, 1973]. This anomaly trends southwest along the Peninsula and south along western Kodiak Island such that the Peninsula volcanoes lie in a region of moderately low crustal velocity to the northwest rather than in this high-velocity anomaly.

6.3. Crustal Faults

[32] Compressional wave velocities across the Denali fault are relatively uniform in the crust and the fault does not show up as a distinctive anomaly in the upper 24 km of the crust. *Brocher et al.* [2004], using TACT refraction profiles, also reported little velocity contrast across the Denali fault zone along the Richardson Highway. The Castle Mountain fault roughly bounds a low-velocity anomaly on its south side, along Cook Inlet and farther east (Figures 6a–6d, 9b, and 9c). With our sparse station array and 25-km node spacing, we would not be able to image narrow low-velocity zones along the active faults. As noted above, the Contact reverse fault forms the southern boundary of a prominent high-velocity feature (Figures 9a and 9b). In Figures 6c and 6d, this high-velocity body can be traced at least 200–250 km along the Contact fault. The Border Ranges fault may similarly form the southern boundary of a velocity low associated with the Copper River basin.

6.4. Subducted Slab

[33] Throughout most of the study area, the subducted slab of the Pacific plate is imaged as a high-velocity anomaly extending to 110- to 190-km depth. The high-

Figure 6. Map views of V_p. Image is masked in gray where there is low resolution. Hypocenters (plus) are shown midway to next slice. Coastline (white), active faults (magenta), volcanoes (triangles), and Mount McKinley (star) are shown. Z equals depth of image in kilometers. For Figure 6i, 110 km depth, the yellow arrows indicate fast direction at 100-km depth from SKS [*Christensen et al.*, 2003]. In Figure 6b, basins are CRB, Copper River; MTB, Middle Tanana; CkI, Cook Inlet. Faults are DF, Denali; TotF, Totschunda; CMF, Castle Mountain; Chug, Chugach Mountains. In Figure 6f, A, mantle expression of STFS. In Figures 6h and 6i, B, low V_p near bend. In Figures 6i and 6j, triangle labeled BC, Buzzard Creek Maar. See Figure 3b for further annotation.

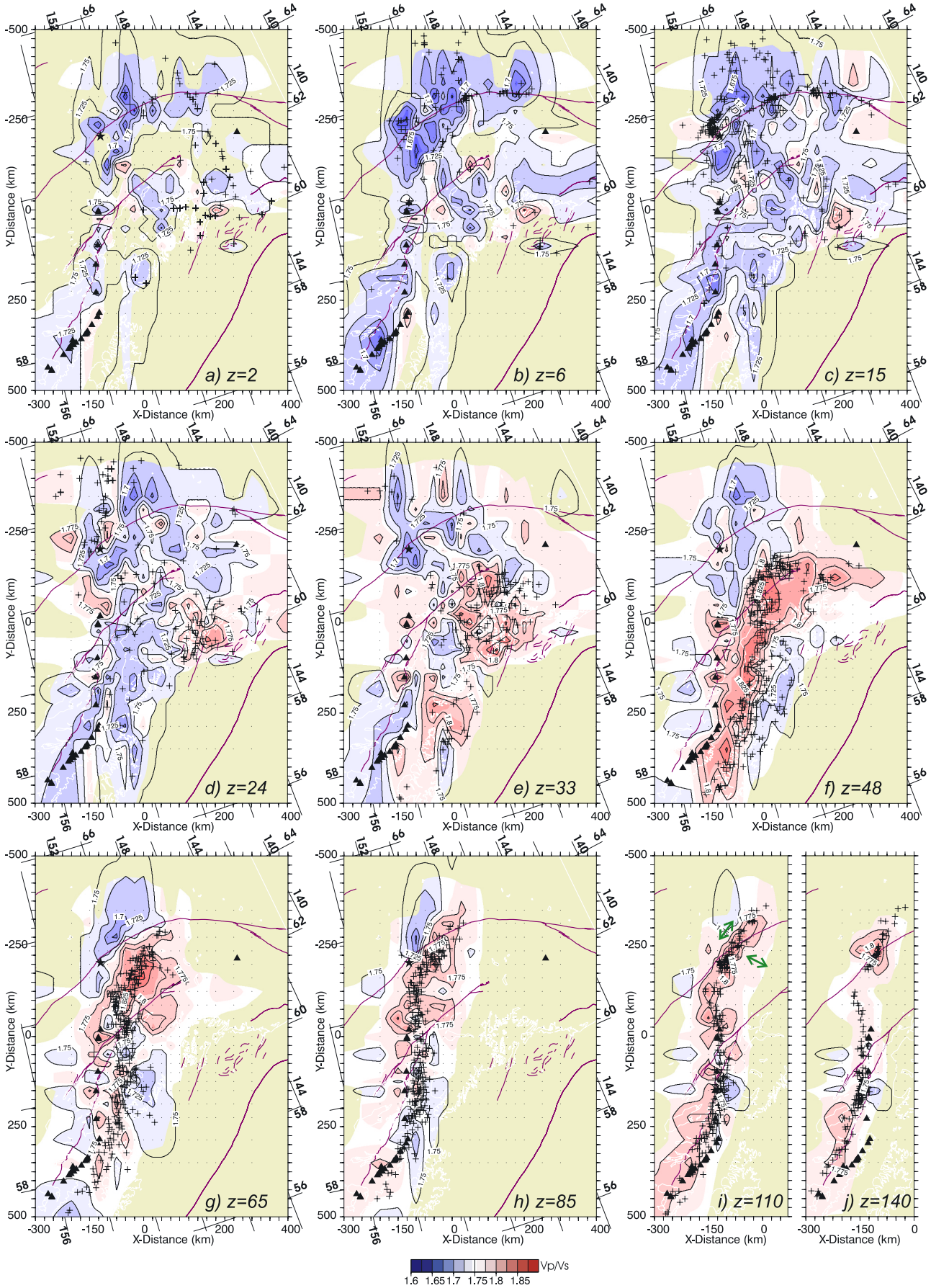
a) z=2
b) z=6
c) z=15
d) z=24
e) z=33
f) z=48
g) z=65
h) z=85
i) z=110
j) z=140
X-Distance (km)
Y-Distance (km)
Vp/Vs
1.6 1.65 1.7 1.75 1.8 1.85

Figure 7

velocity slab is best defined in the central section of our study area, in the vicinity of the Cook Inlet and the Spurr and Redoubt volcanoes (Figures 8a and 8b). This region has adequate resolution, with stations located both west of the volcanoes and east across the Kenai Peninsula. The high-velocity slab is imaged as a roughly 30- to 60-km-thick zone extending to 140-km depth, with a high-V_p core between 8.5 and 8.8 km/s and moderate to elevated V_p/V_s. There is little resolution below the slab so its total thickness is unconstrained. The slab tends to have less pronounced high velocity at depth; however, that result may be due to decreased resolution at depth. At 65-km depth, there are a few nodes with unusually high V_p of 9.0–9.1 km/s (Figure 6g). It may be that the velocity is extra high at those locations, but our preferred interpretation is that the inversion is trying to produce a stronger velocity gradient than would be otherwise possible with our inversion grid spacing.

[34] The high-velocity slab is similar to the previous tomography image of *Kisslinger and Lahr* [1991], but the zone of seismicity is much more tightly defined in our inversion which includes hypocenter parameters in the velocity inversion. *Zhao et al.* [1995] estimated the best fitting uniform high-velocity slab to be 50 km thick, with 8.4–8.6 km/s V_p; and showed strong additional perturbations at 65-km depth. *Searcy* [1996], through inclusion of teleseismic observations, showed that the high-velocity slab extends to 225 km depth, but not deeper than 250 km depth. *Abers and Sarker* [1996] and *Abers et al.* [2006] found from first-arrival traveltimes a 5–8% fast slab in both *P* and *S* at 100–150-km depth (relative to the iaspei91 1-D model [*Kennett and Engdahl*, 1991]). They also infer the presence of a thin (2–6 km) low-velocity channel (3–5% slow) at the top of the slab from body wave dispersion, interpreted as the subducted crust that has not been fully eclogitized at these depths. Such a thin layer is unlikely to be resolved by the data used herein our study, so it is not surprising that it is absent.

[35] In the portion of the subduction zone lying beneath the arc volcanoes, the slab seismicity is generally associated with a sharp velocity gradient at the upper edge of the high-velocity layer (Figures 8a–8d). Thus, from 40- to 190-km depth, the seismicity forms a 10- to 20-km-thick band, defining the top of the slab, with no seismicity in the higher-velocity core of the slab. Because the thickness of the subducting oceanic crust is less than 10 km [*Brocher et al.*, 1994; *Abers and Sarker*, 1996], at least part of the slab seismicity might occur within the upper mantle of the subducting slab, as inferred previously by *Ratchkovski et al.* [1997], who determined a lower zone of earthquakes, separated by 10–15 km from the upper zone and with fewer earthquakes. Along most of the slab, V_p/V_s is higher within the slab, 1.75–1.78, than in the overlying crust (<1.74), as expected for mafic and ultramafic, quartz-free rocks [*Christensen*, 1996; *Hacker et al.*, 2003]. In the segment lying beneath the arc volcanoes, the seismicity also tends to be associated with a gradient in V_p/V_s with lower V_p/V_s within the slab and higher V_p/V_s overlying the slab, again indicating that seismicity lies at the top of the slab (Figures 8a–8d).

[36] In map view, there are two bends in the high-velocity slab, such that the northern and southern sections are subparallel to each other but more easterly striking than the central section (Figures 6g–6h). North of y = −125, it bends sharply toward the east, such that the deep seismicity (Figures 6h–6j) has a corner where the slab bends. South of y = 250, it gradually bends toward the west. While there is less velocity resolution on the southern periphery due to lack of offshore stations, the seismicity also bends gradually. It is intriguing that there is low velocity in the slab mantle, at y = 175, where the southern bend begins (Figures 6i and 8e).

[37] The northern part of the subduction zone shows a different character in the subducted slab and has no associated modern volcanism (Figure 9). The high-velocity slab is apparent, but a distinct low-velocity zone overlies the high velocity. This low-velocity zone is a roughly 20-km-thick layer with V_p < 8.0 km/s to 85-km depth (Figure 9b), exactly as previously imaged by receiver functions [*Ferris et al.*, 2003]. It appears the low-velocity layer may extend to 140-km depth, but there is less resolution at this depth and only a weak broad low is imaged (Figure 9c). This distinct slab layer is even more prominent in the V_p/V_s solution, where it is imaged as a high-V_p/V_s zone, with V_p/V_s 1.78–1.83 from 30- to 140-km depth (Figures 9b and 9c). The seismicity also differs from the subduction zone beneath the arc volcanoes. The northern slab seismicity is located solely within this low-V_p high-V_p/V_s layer rather than at the gradient in V_p or V_p/V_s, as previously observed [*Ferris et al.*, 2003; *Abers et al.*, 2006], and the width of the slab seismicity zone is as narrow or narrower than in the volcanogenic region (Figures 6g and 7g). However, detailed analysis of slab seismicity would require relocating a more complete catalog than our inversion subset.

[38] The exception to a continuous subducted slab is the region east of Cordova (x > 200), where the high-velocity slab extends only about 50-km inland and does not extend deeper than 60-km depth (Figures 6f and 6g). The slab-free region is also the region without deep seismicity (Figure 10c). In the 65-km depth plot (Figure 6g), seismicity is associated with the eastern edge of the high-velocity slab. While there is less resolution to the east where there are no deep earthquakes, there are enough stations that the resolution is adequate, particularly at x = 150, and the lack of high velocity does not appear to be a resolution artifact. Thus rather than a resolution-related reduction in the amplitude of high velocity, there is a decrease in velocity consistent with a slab edge. However, since the resolution drops off below 65-km depth, there is a possibility that the slab extends deeper to the east by dipping more steeply.

6.5. Upper Mantle Wedge

[39] In the volcanogenic subduction zone, the arc upper mantle wedge is imaged as a broad low-velocity region

Figure 7. Map views of V_p/V_s. Image is masked by beige where there is low resolution. Hypocenters (plus) are shown midway to next section. Coastline (white), active faults (magenta), volcanoes (triangles), and Mount McKinley (star) are shown. Z equals depth of image in kilometers. For Figure 7i, 110 km depth, the green arrows indicate fast direction at 100-km depth from SKS [*Christensen et al.*, 2003]. See Figure 3b for further annotation.

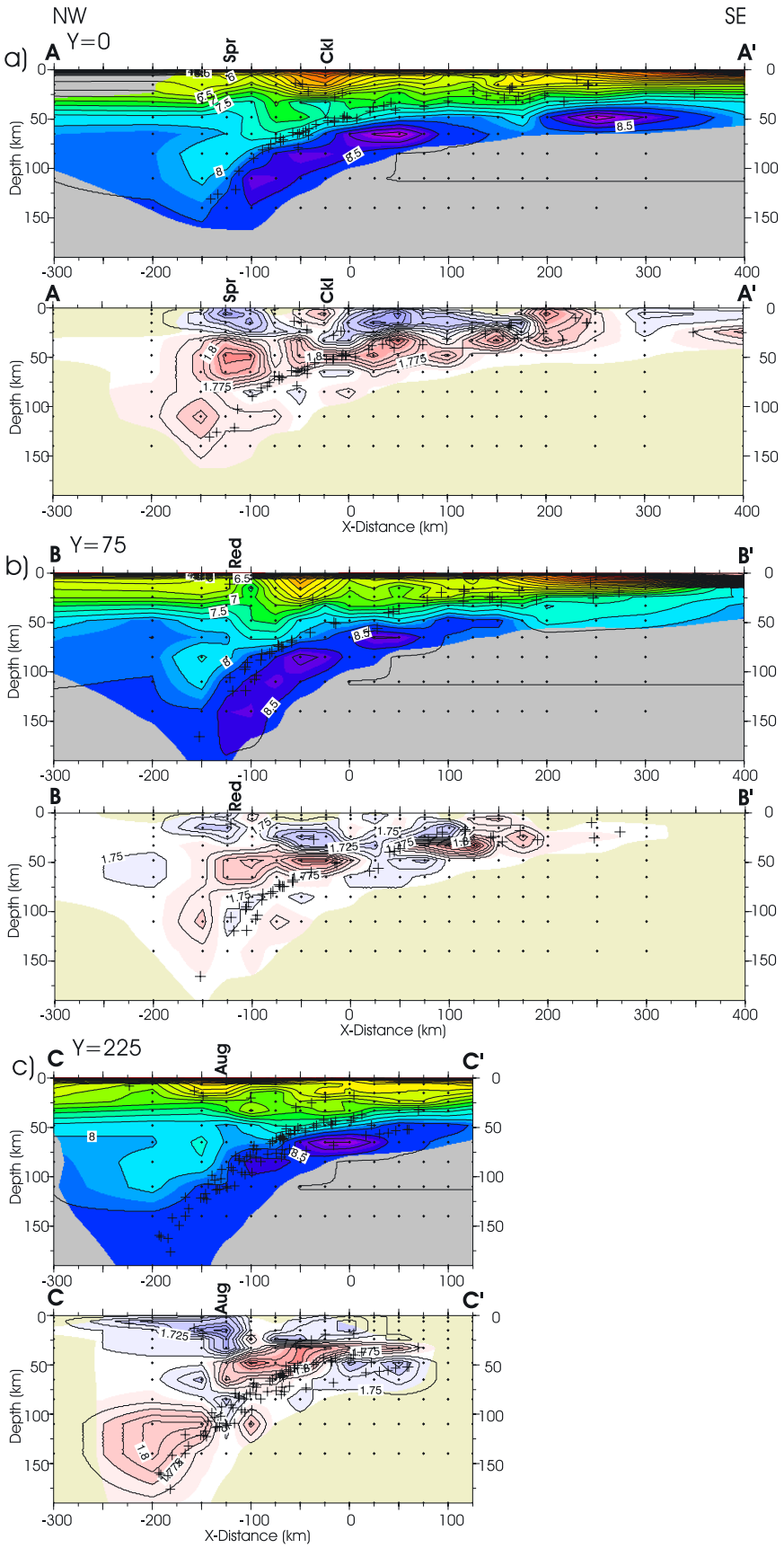

Figure 8. V_p and V_p/V_s cross sections through the Cook Inlet volcanic region, with hypocenters (plus) within 50 km of section. Image is masked where there is low resolution. Spr, Spurr; CkI, Cook Inlet; Red, Redoubt; Aug, Augustine; Kat, Katmai; Ilm, Iliamna. In Figure 8e, B, low V_p near bend.

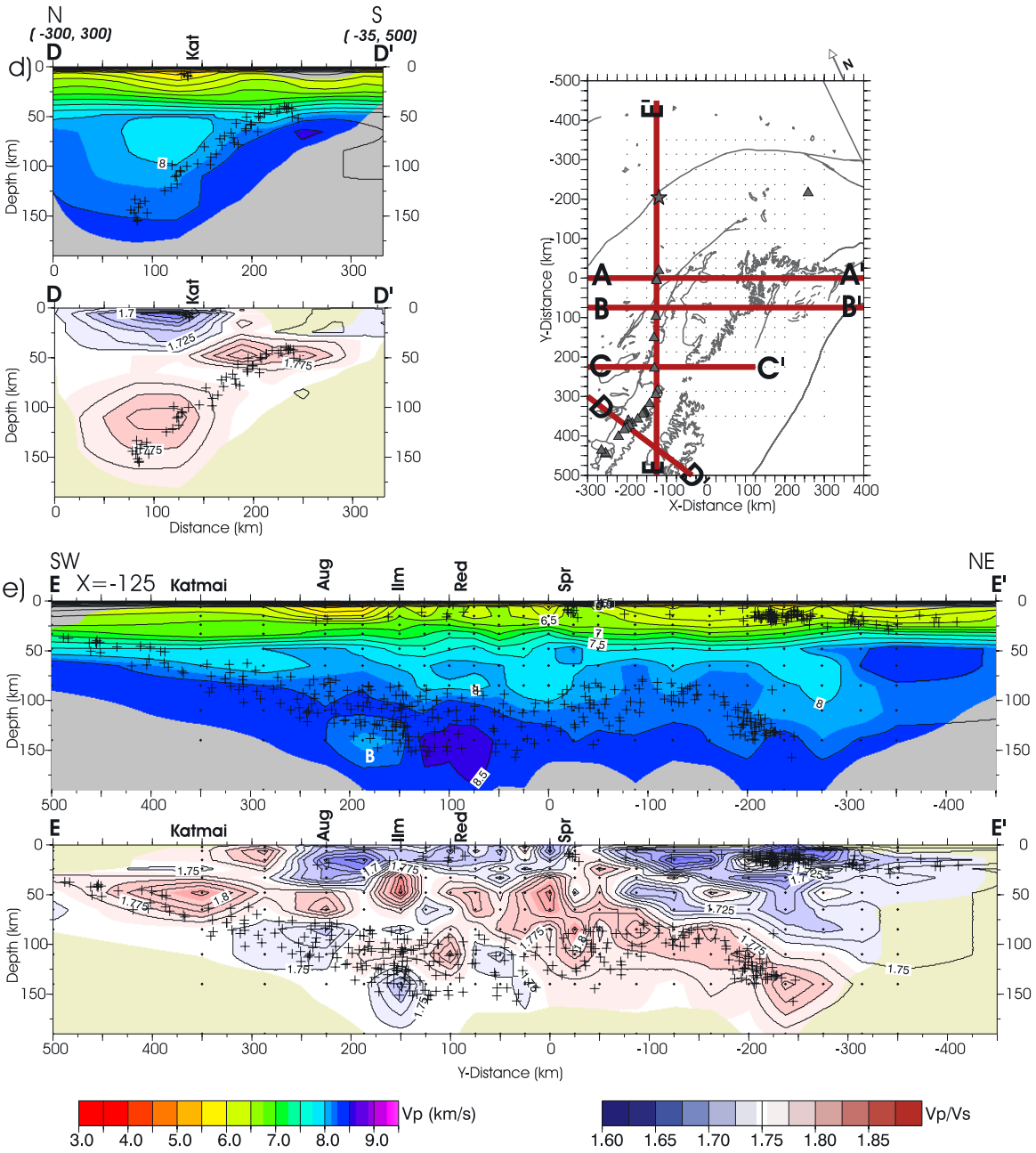

Figure 8. (continued)

overlying the slab from 30- to 110-km depth, with V_p from 6.8 km/s at 30-km depth to 7.8 km/s at 85-km depth (Figures 8a–8e). The mantle wedge low velocity was imaged by *Kisslinger and Lahr* [1991] as a roughly 40-km-wide zone with velocity as low as 7.6 km/s. The mantle wedge is associated with a high V_p/V_s between 1.78 and 1.83. The region of high V_p/V_s is most strongly imaged in the Spurr volcano region and has a well-defined subhorizontal upper boundary at 30 km (Figure 8a), similar to the high V_p/V_s seen in the mantle beneath volcanoes in Japan [*Nakajima et al.*, 2001]. There are lateral variations in V_p/V_s along the volcanic chain (Figure 8e). The resolution of V_p/V_s is relatively uniform along the volcanic chain (Figure 5) and thus the V_p/V_s variations are not artifacts.

[40] In the northern part of the subduction zone, our inversion reveals a different type of mantle wedge. In our V_p/V_s solution, the mantle wedge above the subducted slab is characterized by low V_p/V_s, between 1.68 and 1.72 (Figure 9a), similar to that from receiver functions [*Rossi et al.*, 2006]. The wedge tends to have moderately low V_p, but it is not a broad region of low velocity. There is a small low-V_p region in the region underlying Mount McKinley and extending 150 km to the northeast (Figure 6g), with V_p as low as 7.5 at 65-km depth (A, Figure 9b). However, there is a layer of normal to slightly high-velocity mantle between the mantle low and seismicity associated with the subducted slab, from 33- to 85-km depth (B, Figure 9b). An analogous along-strike variation is seen in the central Andes, where a

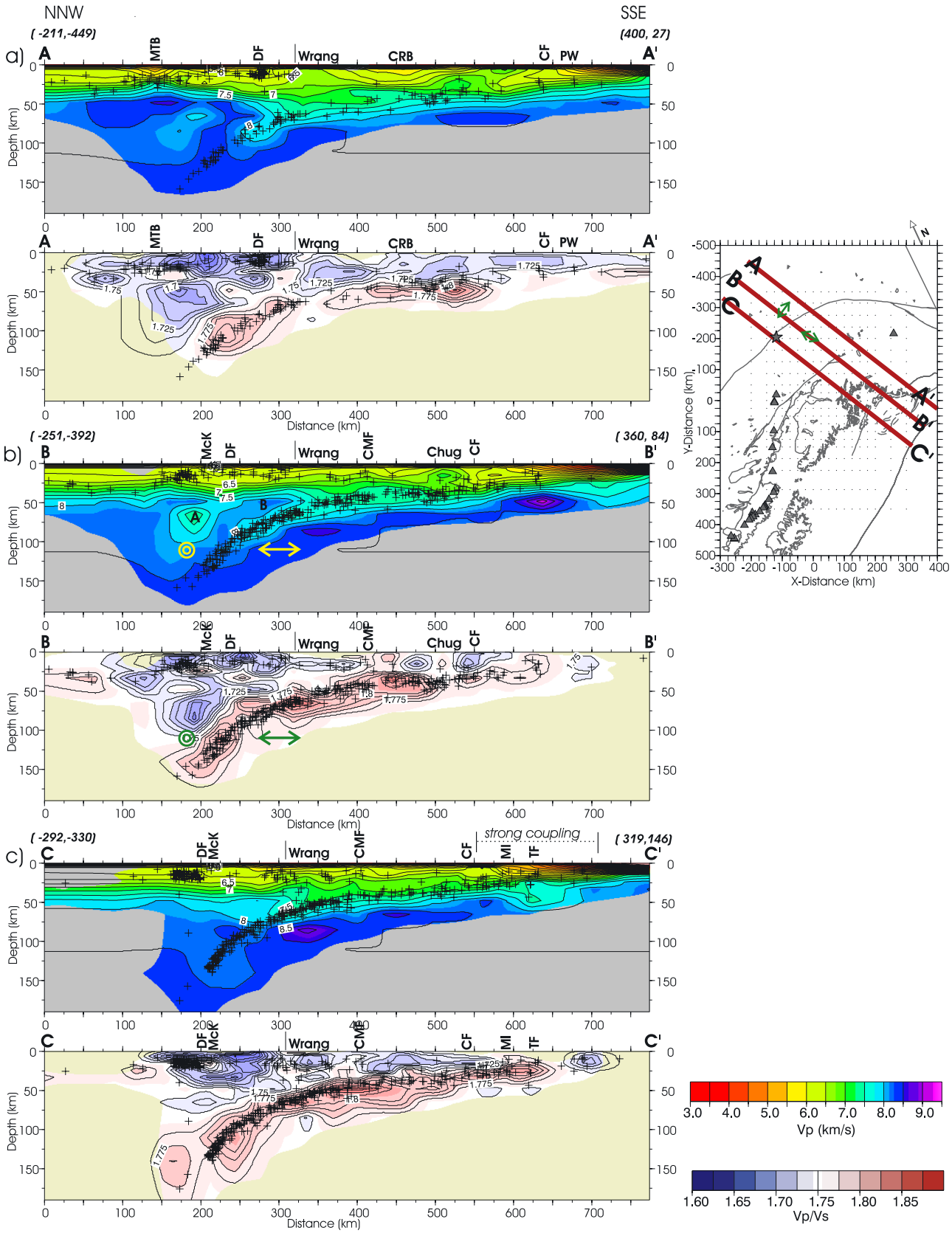
NNW
SSE
(-211,-449)
(400, 27)
a)
A
A'
MTB
DF
Wrang
CRB
CF
PW
Depth (km)
Distance (km)
(-251,-392)
(360, 84)
b)
B
B'
McK
CMF
Chug
(-292,-330)
(319,146)
c)
C
C'
strong coupling
MI
TF
Y-Distance (km)
X-Distance (km)
Vp (km/s)
Vp/Vs

Figure 9

segment with normal dip exhibits a low-V_p, high-V_p/V_s wedge, but the unusual flat slab segment shows low-V_p/V_s in the mantle [*Wagner et al.*, 2005]. There, the low-V_p/V_s wedge also correlates with the absence of volcanism, and is inferred to represent metasomatized mantle converted to orthopyroxenite.

[41] Where the slab is less than 70–90 km deep, the low-V_p, low-V_p/V_s body in the mantle is absent, and instead the mantle has moderate velocities (>8.0 km/s) and V_p/V_s near 1.75 (Figure 9). In the northern segment this region corresponds to a low-attenuation (high Q) region, while Q is uniformly low in the mantle wedge [*Stachnik et al.*, 2004]. Such high-Q forearcs characterize many mantle wedges, and likely reflect low temperatures [*Abers et al.*, 2006].

6.6. Isovelocity Plots and Crustal Thickness

[42] Global and regional variations in crustal thickness are widely used for interpreting tectonics and comparing geophysical data sets [*Mooney et al.*, 1998]. It is valuable to relate our work to that framework. Although the crustal thickness is not directly computed in our velocity inversion because we do not explicitly include a Moho, isovelocity plots can be used to infer variations in crustal thickness. These plots show a contoured surface at a given velocity and can better convey some features than standard slices of V_p. These maps plot the shallowest occurrence of the specified V_p at each grid point, so they do not show low-velocity zones. Also isovelocity is not really a "surface" like a refractor; in fact refractors often are fit with varying velocity. On the basis of our comparison to TACT refraction models, the 7.5 km/s plot is best for conveying a sense of the Moho geometry (Figure 11a). The 2-D TACT profile revealed a 50- to 60-km crustal root beneath the Copper River Basin [*Fuis et al.*, 1991], and a similar root is apparent in the 3-D isovelocity plots.

[43] The region north of the Denali fault, which consists of displaced fragments of North American continental margin [*Plafker and Berg*, 1994], shows a relatively flat transition to mantle velocities at about 40-km depth (Figure 11a). Because upper mantle V_p is generally low south of the Denali fault and above the subducted slab, the V_p contrast at the crust/mantle boundary is low, and the plot primarily shows the shape of the subducted slab, as the mantle velocities are picking up the Pacific plate Moho, from 15 to 70 km depth (Figures 11a and 11b). Note the slab extends deeper and farther north, but it underlies some upper plate mantle. The crust west of the Wrangellia terrane (the Kahiltna overlap assemblage/Farewell terrane) appears to have a higher-velocity upper mantle (Figures 11a and 11b); although the Moho appears to have been perturbed by crustal thickening under the Alaska Range. The odd-looking "depression" offshore (Figure 11a, y = 75, x = 300) is not a deeper Moho, but rather a region of relatively low upper mantle velocity (7.7 km/s) as observed on TACT by *Brocher et al.* [1994] using refraction data.

[44] The reliability of the inferred crustal thickness variations is corroborated by the receiver function study of *Veenstra et al.* [2006] for the McKinley-Denali region BEAAR stations, and *Searcy et al.* [1996] farther north. Their receiver function crustal thickness is most similar in pattern to the 7.5 km/s isovelocity plot (Figure 11a), although 5–10 km thinner. Their greatest inferred crustal thickness is also at the edge of the accreted terranes (A, Figure 11a) where the receiver function also images the subducted slab. Additionally, secondary features are similar in the two methods. For example, both techniques show a less than 100-km-wide area north of the Talkeetna fault with crustal thickness less than 38 km (B, Figure 11a). Farther north, the apparently thinner crust east of Fairbanks (C, Figure 11a) is confirmed by both methods, with receiver functions showing thinner crust, 27–32 km beneath Fairbanks [*Searcy et al.*, 1996] and 25–30 km at BEAAR stations [*Veenstra et al.*, 2006; *Rossi et al.*, 2006].

[45] The isovelocity plots also show features of the subduction zone. For example, a very deep swath in the 7.8 km/s image, in front of the arc and trending in front of the Alaska Range may illustrate the serpentinized forearc wedge. This is roughly the same region where *Stachnik et al.* [2004] image a high-Q zone, which may be cold enough for serpentine to be stable, and where *Blakely et al.* [2005] show a positive magnetic anomaly.

6.7. Comparison to TACT Refraction Profiles

[46] Comparison of our 3-D model to the onshore TACT refraction model [*Fuis et al.*, 1991] reveals important similarities (Figure 12). The refraction model uses refracted and reflected secondary arrivals to estimate layers within the crust. It includes a few PmP arrivals to infer the Moho geometry, and the basic refraction models will have a uniform crust with a sharp velocity discontinuity at the base. The 3-D model only solves for velocity at nodes and does not have layers or discontinuities; and the nodes are relatively coarsely spaced both horizontally and vertically. It only uses first arrivals, but it also includes earthquake sources to 45-km depth in the vicinity of the TACT transect. Thus deeper velocities may be better constrained in the 3-D model because of the earthquakes, but the velocity model will be fairly smooth. For the TACT profile the major crustal velocity features in the two models are similar. The Copper River Basin is imaged as a broad low-velocity feature in both models with $V_p \sim 3.0$ km/s at the surface. The TACT profile defines the base of the basin at a velocity discontinuity between 4.6 and 6.1 km/s at a depth of 5 km. Our inversion defines a comparable basin thickness using a V_p of 4.5 km/s to define the base of the basin. In our inversion, however, velocities as low as $V_p \sim 6.3$ km/s

Figure 9. V_p and V_p/V_s cross sections parallel to Fairweather/Totschunda fault (downdip Yakutat slab), with hypocenters (plus) within 50 km of section. Color image is masked where there is low resolution. In Figure 9b, fast directions at 100-km depth from SKS [*Christensen et al.*, 2003] are indicated by the yellow/green arrows for parallel to the section and by the yellow/green circles for normal to the section; A, unusual mantle low V_p, low V_p/V_s; B, high-V_p shallow mantle. MTB, Middle Tanana basin; DF, Denali fault; Wrang, Wrangellia terrane; CRB, Copper River basin; CF, Contact fault; PW, Prince William terrane; McK, Mount McKinley; CMF, Castle Mountain fault; Chug, Chugach Mountains; MI, Montague Island; TF, transition fault system. The region of strong plate coupling (Figure 2a) is indicated in Figure 9c.

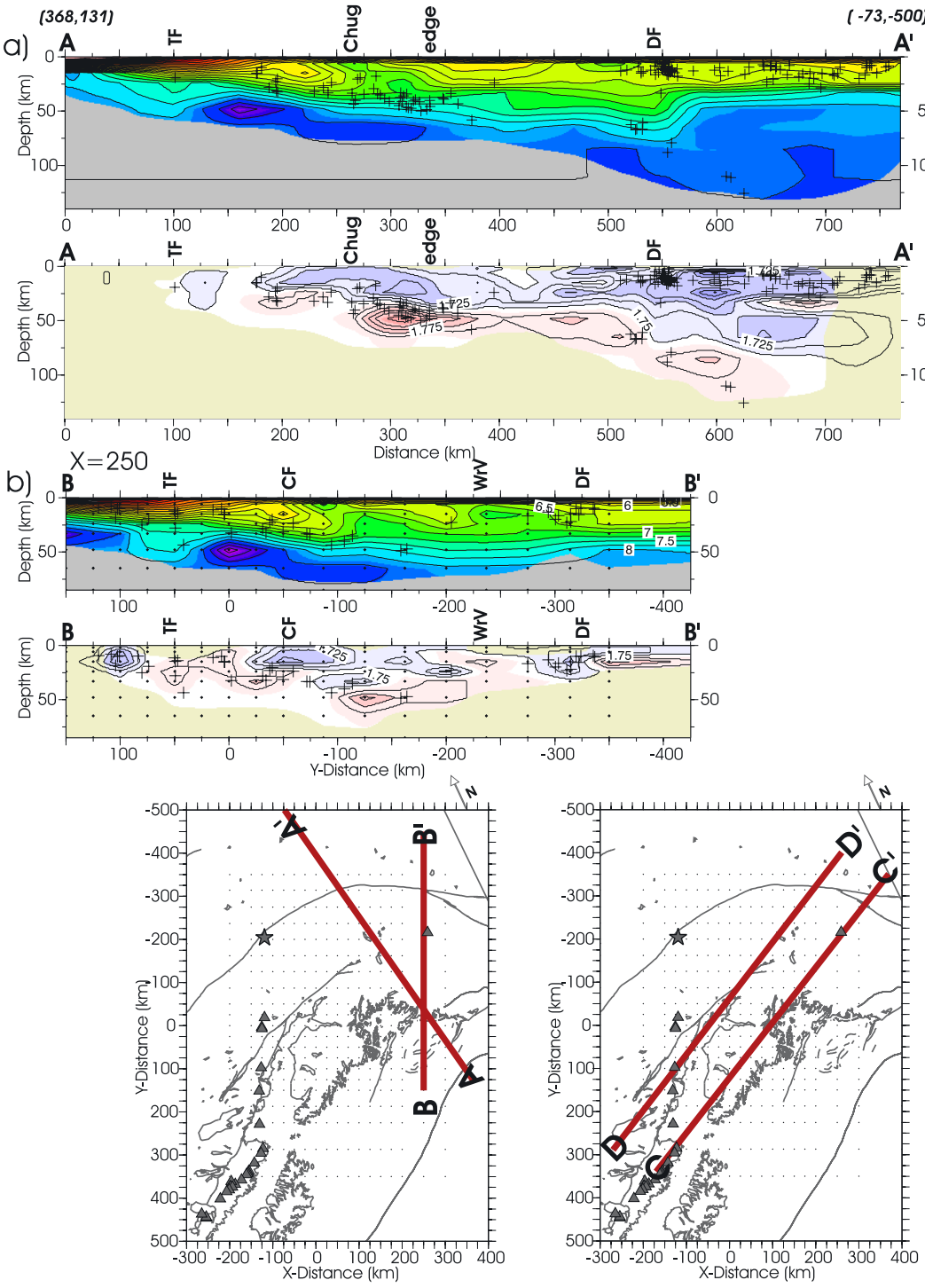

Figure 10. (a, b) V_p and V_p/V_s cross sections normal to central Denali fault, with hypocenters (plus) within 50 km of section. Image is masked where there is low resolution. TF, transition fault system; Chug, Chugach Mountains; DF, Denali fault; CF, Contact fault; WrV, Wrangell volcano; edge, apparent edge of Yakutat slab. (c, d) V_p and V_p/V_s cross sections across the Yakutat slab, with hypocenters (plus) within 50 km of section. Color image is masked where there is low resolution. Spr, Spurr; Red, Redoubt; Aug, Augustine; Ilm, Iliamna; WrV, Wrangell volcano; TotF, Totschunda fault; CRB, Copper River basin; P-Yak, Pacific-Yakutat boundary (STFS).

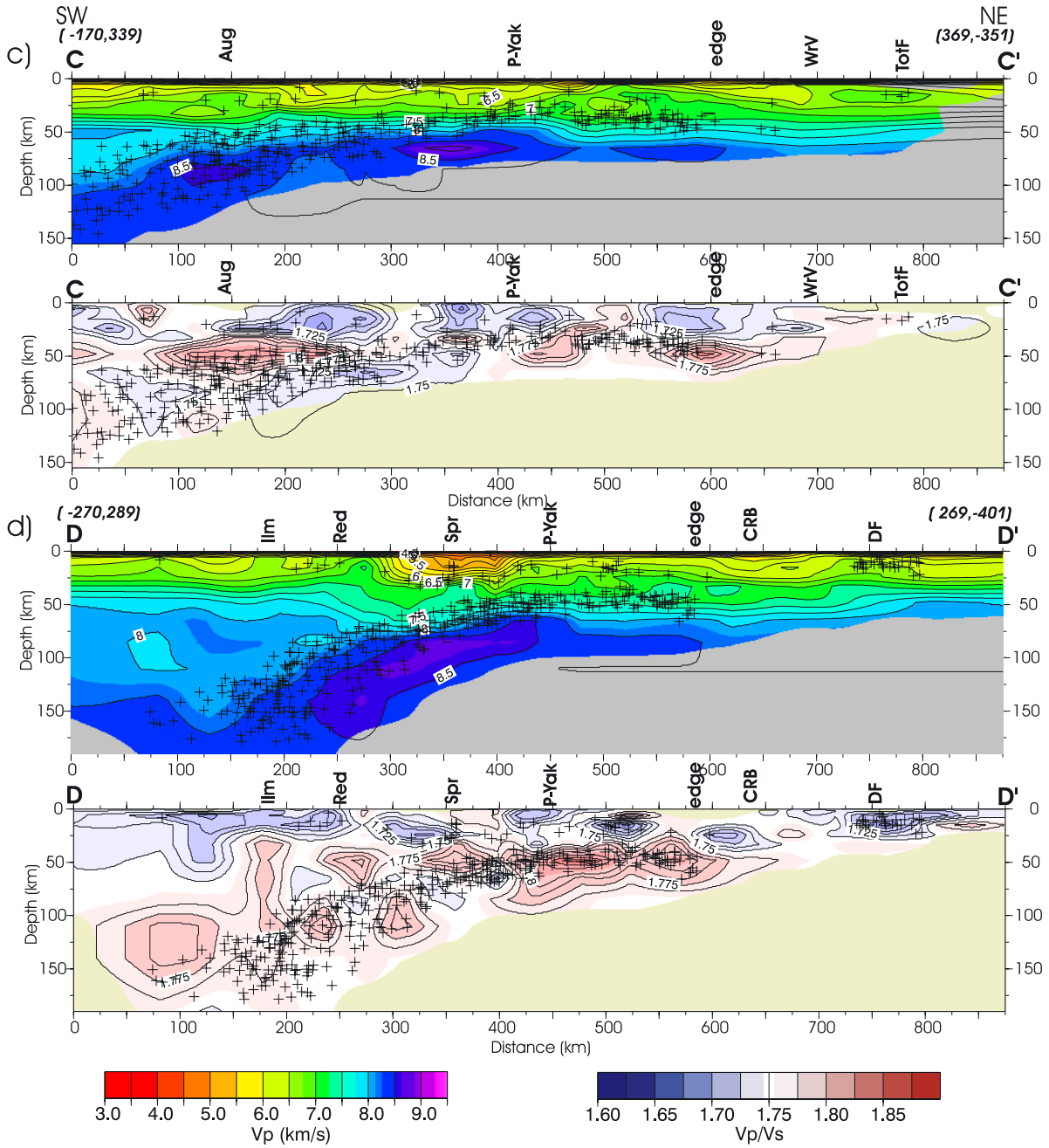

Figure 10. (continued)

extend beneath the basin to as much as 20-km depth. The northern edge of the basin is distinct in our inversion and corresponds to the West Fork fault system. The Contact fault is distinct in both models as the north dipping boundary of the low-velocity crust of the Prince William terrane. The 6.5 km/s contour in the 3-D model is most similar to the refraction model. Using the 7.5 km/s contour in the 3-D model as a proxy for the crust/mantle boundary, based on our comparison of our 3-D model with models for several TACT refraction lines, the general variations in the approximate depth to Moho is similar in both models. Our 3-D model shows a deeper Moho beneath the Contact fault than the refraction model whereas our Moho is shallower beneath the Copper River Basin.

[47] The offshore crustal structure was determined from several TACT refraction profiles by *Brocher et al.* [1994]. Comparison to the 3-D velocity along lines TACT and Kayak is shown in Figure 13, including additional Prince William Sound seismicity [*Ratchkovski et al.*, 2002]. The crustal velocities are similar, with $V_p < 6.0$ to about 15-km depth on the southeast and a sharp change to higher velocities on the northwest that includes a thick 6.9 km/s zone. The 6.9 km/s refractor is inferred to be Eocene oceanic crust by *Brocher et al.* [1994], and the 6.9 km/s velocity material in the 3-D model is similar in depth and orientation, within our resolution. The southeastern offshore edge of this feature appears related to an increase in the seismicity in the subducting slab (Figure 13a, distance

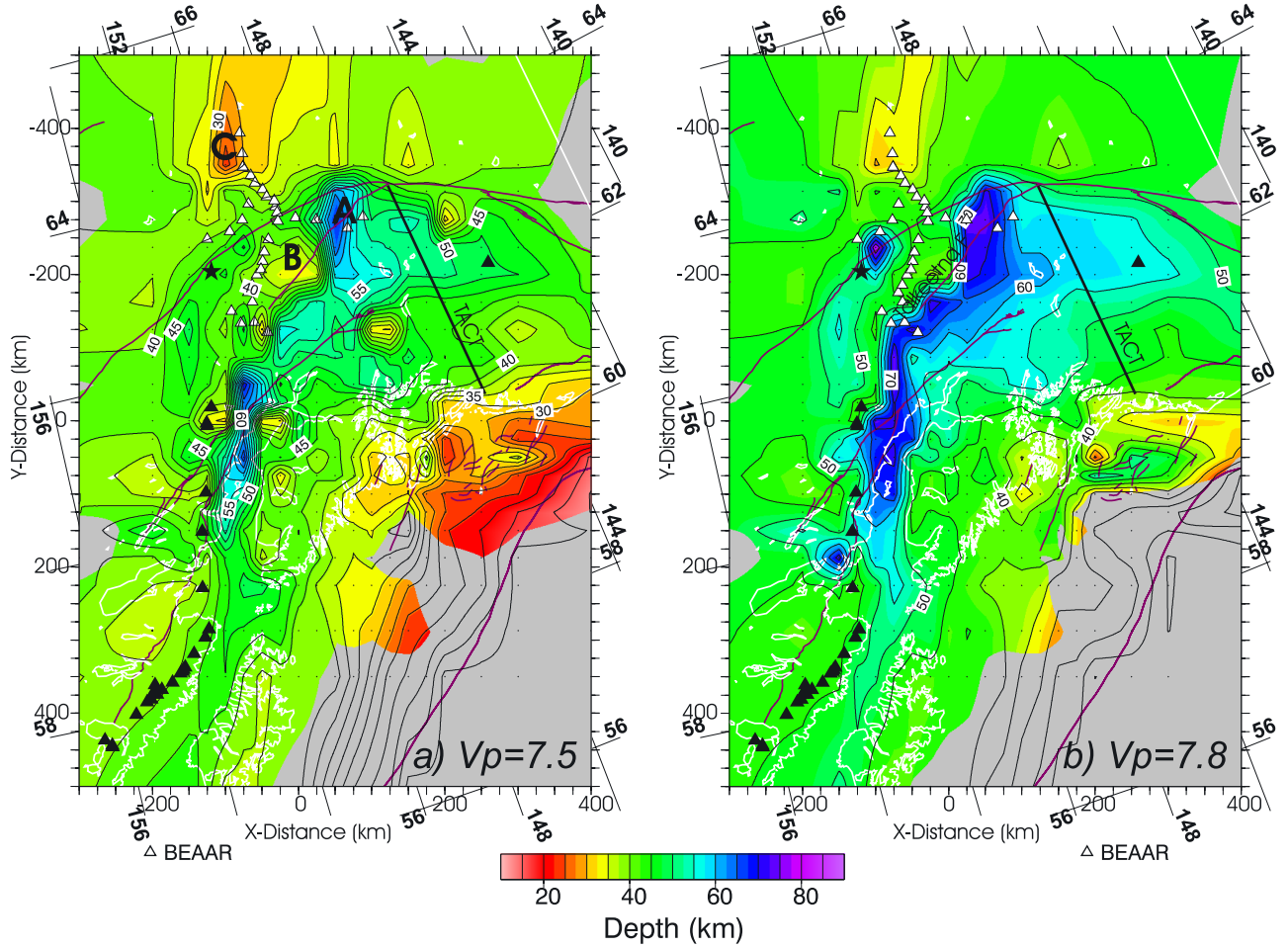

Figure 11. Depth contoured plots of (a) 7.5 and (b) 7.8 km/s isovelocity. Image is masked in gray where there is low resolution. BEAAR stations (white triangles), TACT land profile, coastline (white), active faults (magenta), volcanoes (black triangles), and Mount McKinley (star) are shown. Features A, B, C are discussed in text.

150 km). The offshore mantle V_p in the 3-D model is surprisingly variable, with a region of 7.7 km/s adjoining a region of >8.0 km/s (A, Figure 6f). Such variation was also found in the forward modeling of the refraction profiles with well-constrained mantle V_p of 7.7 km/s along the TACT line (Figure 13a) and 8.0 km/s along the Kayak line (Figure 13b).

7. Discussion

7.1. Subducted Yakutat Terrane

[48] The composition and emplacement of the Yakutat terrane (Figure 2a) are described by *Plafker* [1987] and *Plafker et al.* [1994a], who infer that terrane development began at 48 Ma when the Transition fault system acted as a transform fault at the eastern end of the Aleutian subduction zone. East of the fault, this dextral motion stranded an approximately 200-km-wide nonsubducting section of the Pacific plate plus a fragment of a Cretaceous accretionary prism. At 30 Ma, the Queen Charlotte–Fairweather transform fault formed farther east, allowing the Yakutat terrane between the two transform/transpressional faults to migrate toward the trench and subduct. On the northeastern end of this terrane, subduction of the Yakutat terrane resulted in shortening and uplift of the Chugach–St. Elias Mountains. In this model, about 1200 km of Pacific plate motion has been accommodated along the Transition and Queen Charlotte–Fairweather faults. A portion of the Eocene Transition fault system is mapped at the surface (Figure 2a), and has been extrapolated beneath the Aleutian Megathrust westward by magnetic anomalies [*Bruns*, 1983]. Following *Plafker*'s [1987] model, the fault system must extend farther west within the downgoing subducted slab as the western boundary of the Yakutat terrane. We denote this extensive fault system as the subducted Transition fault system (STFS).

[49] *Plafker* [1987] estimated that 600–1000 km of the Yakutat terrane has been subducted and that Yakutat subduction is responsible for the Wrangell volcanism. He infers that several hundred km of Pacific plate may have subducted under the Yakutat terrane. Currently the Yakutat terrane is moving at close to the velocity of the Pacific plate [*Fletcher and Freymueller*, 2003], but with a more northwesterly azimuth, and thus it has been termed a distinct microplate [e.g., *Pavlis et al.*, 2004].

[50] Our study area includes only the western "oceanic" part of the Yakutat terrane, and not the Cretaceous accre-

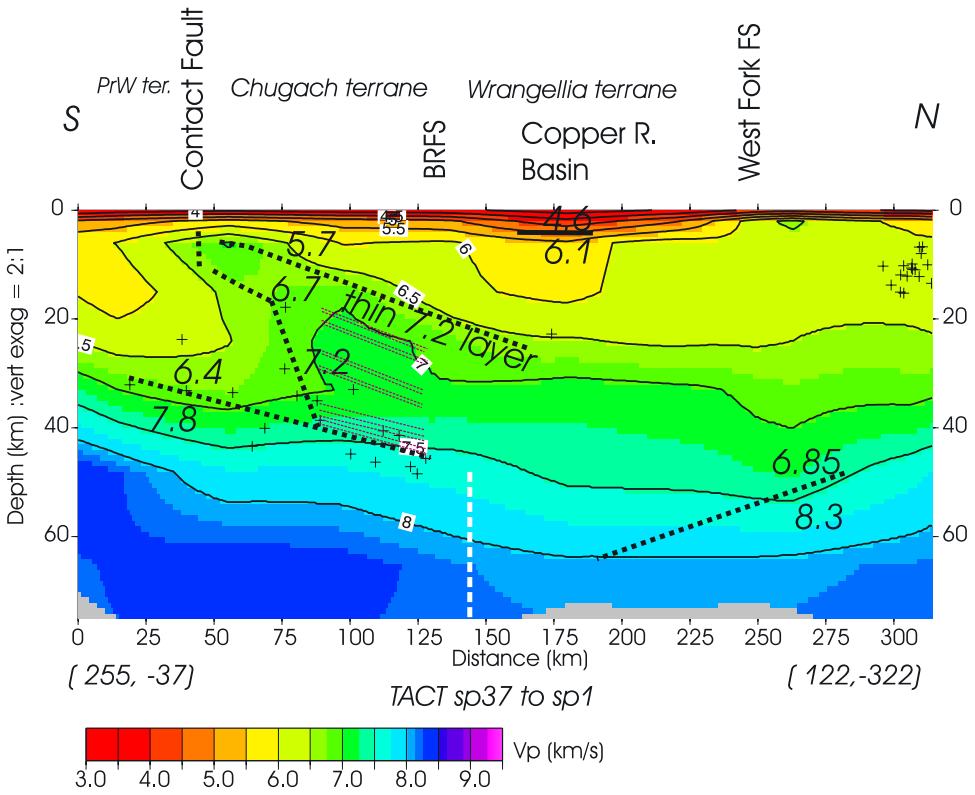

Figure 12. Comparison to main features of onshore refraction model, indicated by heavy line and large numbers [*Fuis et al.*, 1991]. V_p cross section, 2:1 vertical exaggeration, with hypocenters (plus) within 50 km of section. Image is masked where there is low resolution. BRFS, Border Range fault system. Red dashed lines denote sequence of north dipping reflectors seen in parallelogram-shaped region by *Fuis et al.* [1991]. Dashed white line approximates the edge of the Yakutat oceanic slab.

tionary prism rocks forming its eastern margin. The mafic oceanic terrane should be similar to other oceanic subducted plates that generally exhibit crustal seismicity and high-velocity slab mantle, and descend into the asthenosphere as coherent slabs to several hundred kilometers depth. Such characteristics are readily imaged with seismic tomography. Thus we use the term "Yakutat slab" to mean the oceanic part of the Yakutat terrane (Figure 2b). Its thick oceanic crust means that it is not a typical oceanic slab and it may have formed as an oceanic plateau [*Pavlis et al.*, 2004]. Mantle of the continental eastern part of the Yakutat terrane is less likely to form a simple slab since continental rheology results in gravitational instability of the mantle and crustal thickening [*Pysklywec et al.*, 2002].

[51] The Yakutat terrane is associated with relatively low V_p and high V_p/V_s in our 3-D model (Figure 9). Where the terrane is mapped offshore and southeast of Kayak Island, it has low $V_p < 5$ km/s in the upper 6 km, increasing to 7 km/s at 20-km depth (Figure 6). These velocities correspond to the sedimentary cover and the underlying Eocene basalt and oceanic crust. Yakutat slab seismicity is confined to material with $V_p > 6.5$ km/s, which is the basaltic crust (Figure 9). Throughout the region of relatively flat subduction, the uppermost subducting plate has an approximately 20-km-thick section of material with V_p between 6.8 and 7.5 km/s and $V_p/V_s > 1.77$ (Figure 9). This region also contains a 15- to 20-km-thick zone of slab seismicity that forms a relatively smooth surface. The seismic properties of this zone are consistent with thick mafic crust, such as of an oceanic plateau. This is the type of crust inferred for the western half of the terrane by *Plafker* [1987].

[52] *Plafker* [1987] proposed deep subduction of sedimentary rocks. Our results are relatively coarse and would not distinguish such a feature unless it was relatively thick (>5 km) and had a large velocity reduction. Where the Yakutat terrane underthrusts the Prince William and Chugach terranes, in the vicinity of the Contact fault, there is a low-velocity zone dipping under the Chugach terrane (Figure 10b). This represents accretion of underthrust sedimentary rocks within the overlying plate.

[53] The low-V_p, high-V_p/V_s feature associated with the Yakutat terrane subducted slab extends to the 110- to 140-km depth (Figures 9a and 9b). Thus the Yakutat terrane has subducted to at least 140-km depth (the depth of the deepest seismicity in the northern subduction zone). The low-velocity subducting plate was also imaged with receiver functions by *Ferris et al.* [2003]. Their waveform inversion shows an 11- to 22-km-thick low-velocity zone at the top of the slab to 150 km depth, up to 20% slower than surrounding mantle. They show that this requires about 600 km of subduction from the Aleutian trench, which is consistent with *Plafker*'s [1987] tectonic reconstruction. From our results we infer the western edge of the Yakutat slab as shown in Figure 2b, with an uncertain amount of Pacific plate underthrust. This can be compared to map views (Figures 6, 7, and 11).

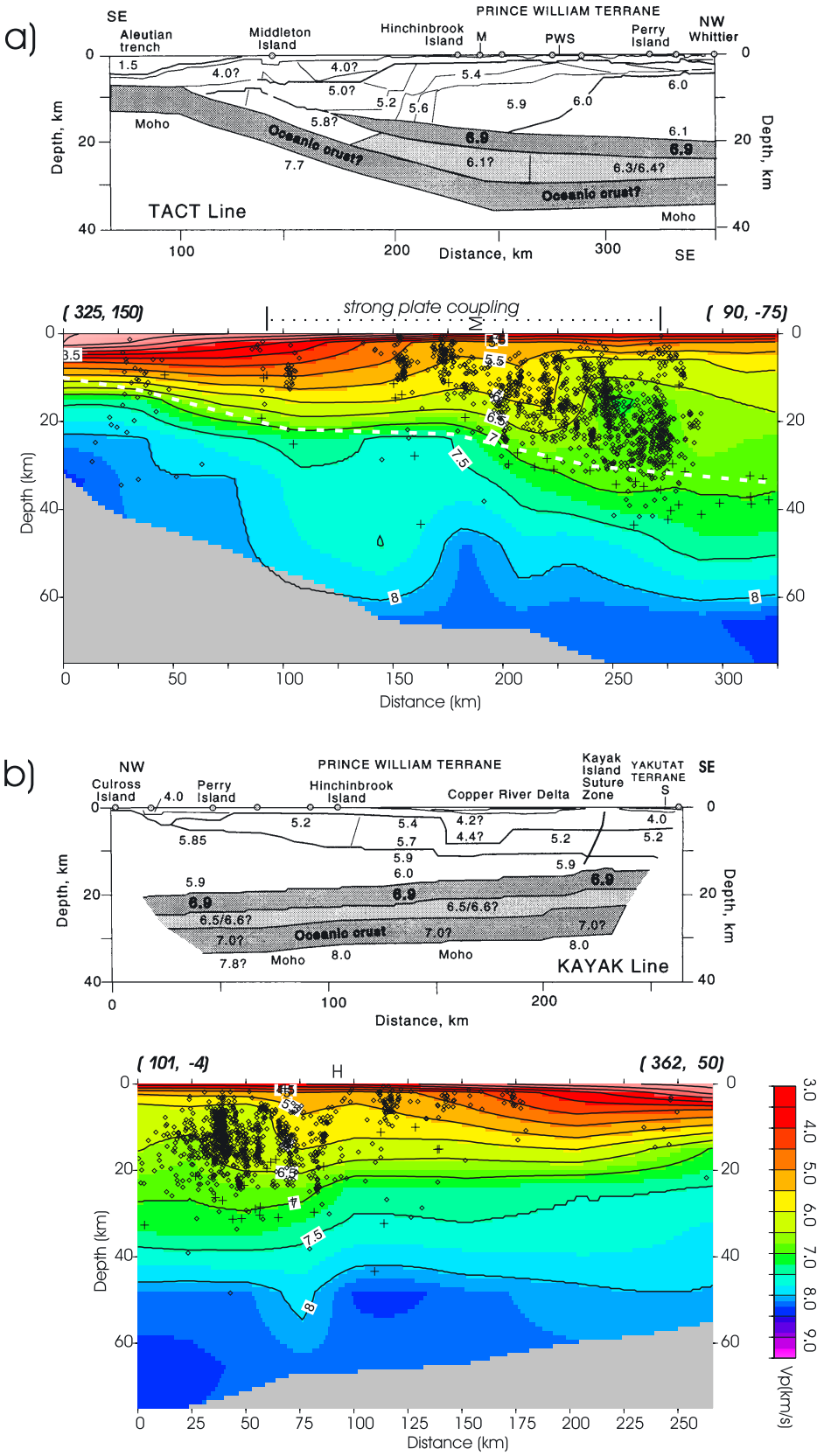
a)
SE
PRINCE WILLIAM TERRANE
NW
Aleutian trench
Middleton Island
Hinchinbrook Island
M
PWS
Perry Island
Whittier
Depth, km
Moho
Oceanic crust?
TACT Line
Distance, km
SE
(325, 150)
strong plate coupling
(90, -75)
Depth (km)
Distance (km)
b)
NW
PRINCE WILLIAM TERRANE
Kayak Island Suture Zone
YAKUTAT TERRANE
SE
Culross Island
Perry Island
Hinchinbrook Island
Copper River Delta
Oceanic crust
Moho
KAYAK Line
Distance, km
(101, -4)
H
(362, 50)
Depth (km)
Distance (km)
Vp(km/s)

Figure 13

[54] The western edge of the subducted Yakutat terrane should show an abrupt change in crustal thickness across the STFS, as seen in seismic reflection profiles [*Fisher et al.*, 2005]. This offset is seen in the 7.8 km/s isovelocity plot (Figure 11b) where there is northwest trending feature with approximately 10 km thicker crust on the northeast (interpretation shown on Figure 2b). In cross sections across the top of the subducting plate (Figures 10c and 10d), the seismicity defines a relatively smooth top of the subducting plate across the edge of the Yakutat terrane (labeled P-Yak). The subducting Transition fault is inferred to be an old oceanic strike-slip fault that separates different types of crust with different thicknesses, but the combined Pacific plate and western part of the Yakutat terrane seem to be subducting together, as there is no sharp change in seismicity that might be expected for a tear.

[55] Following this trend offshore to the southeast is the area with relatively low velocity at 33- to 48-km depth (Figures 6e and 6f; labeled "A"), which may also be a signature of the STFS. East of Montague Island, the STFS is imaged with low velocity below 30 km. This characteristic may be best explained by the partial subduction of Pacific plate under Yakutat as suggested by *Plafker* [1987]. Thus, in cross section (Figure 10b), the broad low velocity (under "TF", at y = 50) may be a region of doubled oceanic crust and the high velocity at 48-km depth to the north may represent the upper mantle of the Yakutat slab, under which the Pacific plate has partially subducted. This would suggest 50–100 km of Pacific-Yakutat subduction, although the amount is poorly constrained by our coarse 3-D model, which has a sharp drop in resolution southward (Figures 4e and 4f). The abrupt western end of the low-velocity feature (Figure 6f) may be related to some preexisting structure on the STFS such as a short ridge segment from *Plafker*'s [1987] tectonic model. *Brocher et al.* [1994] found a similar region of lower-velocity mantle (7.7–7.8 km/s) subparallel to the Transition fault.

[56] The apparent northeastern edge of the subducted Yakutat oceanic terrane is imaged as the edge of the high V_p/V_s and underlying high-V_p slab, and the edge of the deep seismicity (>50 km), as seen in the 48- to 65-km depth map views (Figures 6e, 6f, 7e, and 7f). The northeastern edge is most apparent in cross sections parallel to the strike of the slab (Figures 10c and 10d). The slab seismicity ends abruptly above the edge of the 65- to 85-km-deep high-velocity layer (Figures 10c and 10d, under label "edge"). The edge is not simply a tapering off of resolution, and the mantle velocity east of the Yakutat slab has decreased from the initial model. The apparent slab edge can also be inferred from the TACT profile, as the end of a feature that produces reflected arrivals in wide-angle data and a 5-km-thick band of reflections in seismic reflection data (Figure 12) [*Fuis et al.*, 1991].

[57] The apparent northeastern edge is drawn as the Yakutat slab edge in Figure 2b. With such an abrupt change in seismicity and material properties, this most likely represents the edge of the Yakutat Eocene volcanics, which may be oceanic plateau. However, we cannot rule out the possibility that additional Yakutat material extends farther east and deeper, because our resolution decreases with depth (Figure 10d.) *Fuis et al.* [1991] consider that slab material extends farther north of the boundary sketched in Figure 2b but dips sharply steeper.

[58] *Page et al.* [1989] located four magnitude 2–3 earthquakes greater than 75 km deep in the Wrangell region during the period 1971–1986 and denoted a Wrangell Wadati-Benioff zone with a slab subducting northeastward. This orientation is roughly normal to the direction of plate motion. For our velocity inversion, we include only well-constrained earthquakes magnitude >2.5, from 1991 to 2002 and did not find any events this deep in the Wrangell region; and 3-D relocation of the entire catalog, 1971 to present, has not yet been undertaken. However, occasional small-magnitude deeper earthquakes are observed in regions of crustal thickening [*Kohler and Eberhart-Phillips*, 2003] and do not necessarily indicate continuous subducted oceanic plate. Even if subducted Yakutat material extends farther or deeper toward the northeast, it is still primarily a passive edge of the large slab that is subducting northwestward (Figure 2b).

[59] East of the Aleutian trench subduction, the Yakutat deformation changes to oblique convergence dominated by uplift of the St. Elias orogen with formation of a 400-km-long, 70-km-wide region of high topography (Figure 2a) [*Pavlis et al.*, 2004]. This high-topography region is northeast of the Yakutat slab. In the 3-D model, it is associated with the region of thick crust between the Yakutat slab and the Denali fault (Figures 10d and 11). The region of crustal thickening is also shown in Figure 2b. Note that the resolution drops off toward the eastern periphery, and it is possible that the region of crustal thickening could continue to the southeast along with the high-topography region. However, it is also feasible that the crustal thickening is more pronounced on the west than the high topography, as implied in the 3-D image. Lower crustal rheology allows lateral extrusion such that crustal thickening need not be directly located under crustal uplift [*Gerbault et al.*, 2002], and in many convergent mountain ranges elastic plate strength causes offset between roots and the highest topography [e.g., *Molnar and Lyon-Caen*, 1988]. From the 7.5 km/s contour (Figure 11a), the crust thickens to approximately 50 km, which is similar to that estimated from wide-angle reflections by *Fuis et al.* [1991] (Figure 12).

7.2. Relation Between Pacific Plate and Yakutat Slab

[60] The 3-D velocity does not provide specific Pacific-Yakutat displacements, but because it images the entire subducted slab, it provides some useful insights/constraints. In a 2-D model, the Yakutat slab is a small microplate and tectonic models based on observed surficial bounding faults

Figure 13. Comparison to onshore-offshore refraction models [*Brocher et al.*, 1994] for (a) TACT and (b) Kayak lines (see Figure 3a). V_p cross sections, 2:1 vertical exaggeration. Image is masked in gray where there is low resolution. Hypocenters within 25 km of section: plus, inversion earthquakes; diamond, double-difference 1-D relocations of seismicity from *Ratchkovski et al.* [2002]. The region of strong plate coupling (Figure 2a) is indicated in Figure 13a. Dashed white line shows approximate location of the plate interface, which is not specified in the 3-D velocity model.

may result in interpretations that are inconsistent with the extensive subsurface subducted slab. In the mantle, we consider that the Yakutat slab is subducting with the Pacific plate and is not moving independently as a truly distinct plate. However, its properties result in Pacific/Yakutat relative displacement at shallow depths.

[61] It is thicker than normal Pacific oceanic crust, and hence more buoyant, explaining why mountain building occurs only where Yakutat crust subducts [*Ferris et al.*, 2003]. This means the descending slab dips more shallowly. If the Yakutat slab is descending more shallowly, but is welded to the more steeply dipping Pacific plate, this could naturally lead to a small amount of relative displacement at the Earth's surface where the two sections have the same dip (i.e., where have not yet subducted).

[62] Thus, within the viscous mantle, we presume there would be little reason for deformation between the sections of subducting slab since the primary force would be slab pull of the large subducting Pacific plate, and the mantle component of the subducting Yakutat plate. As both kinds of crust metamorphose to eclogite, probably near 150 km depth here [*Abers and Sarker*, 1996], the metamorphosed crust also adds negative buoyancy [*Hacker*, 1996]. At shallower depths, as the subducting Pacific plate pulls the more buoyant Yakutat slab downward, the Yakutat slab overthrusts the shallow Pacific plate as a secondary effect. We infer this secondary effect is what is measured with surface deformation observations.

[63] Alternatively, if there were no shallow Pacific-Yakutat relative displacement, then there would be a tear between the sections of subducted slab. We do not image such a tear in the slab, although a gradual bend may be present. Consider Figure 6h (85-km depth) which shows a distinct bend, but the slab is a continuous high-velocity feature and the slab seismicity is continuous. Also, if the Yakutat terrane was attached to the Pacific plate at the surface, the northeastern edge of the Yakutat terrane should lie northeast of the Totschunda fault, based on the Pacific–North America relative plate motions in southern Alaska, which have become more clockwise through time (Figure 2b). However, this is not the case, but rather the inferred northeastern edge of the Yakutat terrane lies roughly 150 km to the southwest (Figure 2b). Thus the surficial Yakutat terrane has been moving relative to the Pacific plate for a long time.

[64] Our 3-D interpretation may convey apparently conflicting descriptions of relative motion depending on the viewpoint. From the viewpoint of the entire Yakutat slab, the slab is subducting together with the Pacific plate. However, in the more common viewpoint of only the portions of plates that are observed at the Earth's surface, the Yakutat block is moving relative to the Pacific plate, as measured geodetically (Figure 2a).

[65] As mentioned previously, the geodetic data indicate the Yakutat terrane is moving at close to the velocity of the Pacific plate, but in a more northwesterly direction [*Fletcher and Freymueller*, 2003]. Geologic mapping and structural interpretations also support the idea that the Yakutat terrane is being shoved westward just south of the Chugach–St. Elias thrust [*Pavlis et al.*, 2004; *Bruhn et al.*, 2004]. The fact that the northeastern edge of the subducted Yakutat slab (Figure 2) lies southwest of the line between the Fairweather fault and the Totschunda fault suggests that these indications of relative motions between the Yakutat terrane and the Pacific plate represent a long-lived process, perhaps since the initiation of the Yakutat terrane collision around 25 Ma. *Plafker* [1987] and *Fletcher and Freymueller* [1999] suggested the Transition fault may accommodate this deformation, in that it was initially a transform fault, but it is now a low-angle thrust. Our results do not constrain the extent of underthrust Pacific plate and the amount of sketched overlap is schematic (Figure 2b).

7.3. Terranes of the Overriding Plate

[66] South of the Denali fault, southern Alaska is composed of a series of terranes accreted prior to mid-Cretaceous time (Figures 1 and 2; for comparison of features, note that the rectangle in Figures 1 and 2 corresponds to the velocity plots in Figures 6 and 7). These terranes exhibit differences in velocity among themselves and are different from the preexisting North American continent, north of the Denali fault (see Figure 1). If V_p of 7.5 km/s is considered a rough estimate of crustal thickness (Figure 11a), there is a distinct change in crustal thickness across the central Denali fault, yet west of x = 0, the gradient in crustal thickness follows the northern boundary of the Wrangellia terrane (Talkeetna fault) rather than the western Denali fault. This suggests that the accreted terranes do not have their own mantle and is consistent with ideas of subsequent underplating [*Fuis and Plafker*, 1991] or that crust has been subsequently deformed by reactivating terrane-bounding faults.

[67] The accreted terranes tend to exhibit slightly higher crustal V_p than the para-autochthonous terranes of North American continental affinity, which have $V_p < 6.5$ km/s in the upper 25 km (Figures 6c and 6d). There is also a distinct change in V_p/V_s such that the continental crustal rocks have lower V_p/V_s, <1.7 (Figures 7b and 7c). These differences can be explained by the common presence of intermediate to mafic volcanic rocks and sediments in the Wrangellia and Peninsular terranes, south of the Denali fault, whereas the continental margin terranes north of the Denali fault consist dominantly of more felsic metasedimentary rocks [e.g., *Plafker et al.*, 1994a].

[68] The younger Prince William terrane has relatively lower velocity than the older, more inboard terranes, with $V_p < 6.5$ km/s in the upper 20 km (Figure 9b). This terrane consists of Paleogene sedimentary rocks, and interbedded volcanics and granitic plutons. The velocity contrast makes the terrane bounding Contact fault apparent where the Prince William terrane underthrusts the older Chugach terrane. There is also scattered seismicity in the vicinity of the thrust boundary zone. This finding is remarkable in light of geologic studies from western Prince William Sound indicating no significant difference in the structure or sedimentology of the rocks on either side of the inferred trace of the Contact fault [*Bol and Gibbons*, 1992; *Dumoulin*, 1988]. The Contact fault in eastern Prince William Sound is much more pronounced [e.g., *Bol and Roeske*, 1993], and geophysical differences across the structure are expected.

[69] The Wrangellia and Chugach terranes generally have $V_p \geq 6.5$ km/s at 15-km depth (Figures 6c and 9c). This velocity is reasonable for the metasedimentary and metavolcanic rocks [*Christensen and Mooney*, 1995]. The Wrangellia terrane also includes underlying Talkeetna arc rocks

that show a largely mafic bulk composition [*DeBari and Sleep*, 1991]. The Wrangellia terrane is characterized by a relative absence of upper crustal distributed seismicity compared to the adjacent North America continent and Peninsular and Chugach terranes (Figures 1, 6b, and 6c). The relatively aseismic character may be the result of different rheological properties.

[70] The Kahiltna flysch terrane is described by *Plafker and Berg* [1994], *Stanley et al.* [1990], and *Ridgway et al.* [2002]. It is a Mesozoic flysch sequence that formed in an ocean basin on the northern margin of the Wrangellia terrane. Cretaceous oblique subduction collapsed the basin and imbricately sheared and underthrust large volumes of schist under the Yukon-Tanana terrane. *Stanley et al.*'s [1990] magnetotelluric surveys showed very conductive rocks to at least 20-km depth, which are most likely carbonaceous shales of the Kahiltna flysch. At greater depth, increased metamorphic recrystallization is interpreted to reduce conductivity and the ability to detect the flysch.

[71] In the crust, the Kahiltna flysch terrane is characterized by relatively low V_p (<6.5 km/s to 24-km depth, Figure 6d) and low V_p/V_s (<1.7, Figure 7b), such that the boundary with the Wrangellia terrane is apparent (see lab measurements of *Brocher et al.* [2004]). Below 33-km depth, a feature appears in the tomography that can be interpreted as the Cretaceous subduction of underthrust Kahiltna flysch, seen in Figure 9b as a north dipping low-V_p zone to the north and overlying the Yakutat slab separated by a high-velocity zone. This is also seen in the 65-km depth map view (Figure 6g) where a low-V_p anomaly extends northeast of Mount McKinley and the Denali fault, with V_p as low as 7.0 at 65-km depth. We interpret the low-V_p feature as representing the underthrust leading edge of Wrangellia emplaced during Cretaceous collision, perhaps with a thick section of metamorphosed Kahiltna flysch. The underlying adjacent high-velocity layer (B, Figure 9b) may represent a portion of the subducted oceanic slab that transported the flysch, metamorphosed to eclogite, or an intervening piece of mantle. In V_p/V_s, the low-V_p feature is characterized by low V_p/V_s (<1.7) in contrast to the Yakutat slab. Similar low V_p/V_s for this part of the mantle have been inferred from receiver functions [*Rossi et al.*, 2006]. Low V_p/V_s may reflect a high quartz content, which has a very low V_p/V_s [*Christensen*, 1996]. *Brocher et al.* [2004] report low V_p/V_s of less than 1.7 for some quartz-rich Yukon-Tanana terrane rocks.

[72] Any metasediment subducted to depths of 65 km (>2 GPa pressure) would undergo substantial metamorphism, probably to garnet-granulite facies. At these conditions, seismic velocities can be quite high depending upon bulk composition [*Rudnick and Fountain*, 1995; *Behn and Kelemen*, 2003]. The bulk composition of clasts comprising the Kahiltna flysch are described as andesitic [*Stanley et al.*, 1990] although variable spatially [*Ridgway et al.*, 2002], and potentially modified by metasomatism, so it is unclear what such rock would look like following subduction. The one constraint is the low V_p/V_s, which likely requires that quartz be abundant as sometimes seen in exhumed high-grade rocks [*Liou et al.*, 1998]. Quartz is the only common mineral that might be stable at mantle conditions and which has $V_p/V_s < 1.73$ [*Christensen*, 1996; *Hacker et al.*, 2003]. At pressures above 2.5–3 GPa (60–85 km depth), quartz will convert to coesite [*Akaogi et al.*, 1995]. In order to remain in the mantle for the approximately 110 Myr since arc accretion, some process would have to isolate these rocks from mantle flow associated with subsequent subduction. High temperatures have been inferred for this portion of the mantle wedge from seismic attenuation [*Stachnik et al.*, 2004], so it is likely that these rocks are weak enough to flow (particularly if quartz rich), but buoyancy may limit mobility.

[73] In the terranes north of the Denali fault, there is one unusual feature in the 3-D model. Near x = −100, y = −350, there is a 50- to 100-km-wide northeast trending region with shallow low velocity, 5.4 km/s at 6-km depth, underlain by high velocity, 7.5 km/s at 24-km depth (MTB, Figures 6a–6d and 9a). The shallow low velocity represents the Middle Tanana basin [*Ehm*, 1983], which is characterized by a prominent 25 mGal isostatic gravity low [*Frost et al.*, 2002] and strong reverberations in receiver functions [*Veenstra et al.*, 2006; *Rossi et al.*, 2006]. Sedimentary cover inhibits accurate mapping of the basement rock in this part of the Yukon-Tanana terrane and identification of the underlying high-velocity rock. However, *Stanley et al.* [1990], in a magnetotelluric profile, inferred a large body of resistive rock (>1000 ohm m) from 5 to 20 km depth in this region. Stanley infers that it represents high-grade schist. Some mafic terrane fragment would be another possibility. There is abundant seismicity associated with the high-velocity crust, although it appears to be part of a larger region of distributed seismicity.

7.4. Subducted Pacific Plate

[74] The subducted Pacific plate is imaged as a high-V_p slab to 110–190 km, along the 600 km of the subduction zone southwest of the subducted Yakutat slab (Figures 6g and 8a–8d). However, there is one intriguing low-velocity feature that departs from the uniform character of the slab. At y = 150 km, the V_p of the slab mantle is low from 65- to 140-km depth, to 7.9 km/s at 110 km (labeled "B", Figures 6h, 6i, and 8e). This is the location south of Cook Inlet where the slab bends to become more parallel to the trench. There could be some preexisting structural feature of the incoming Pacific plate that is related to the low V_p. For example, the Kodiak-Bowie seamount chain impinges upon the trench just south of this feature [e.g., *Silver et al.*, 1974] (Figure 2b). Seamounts, or sediments trapped in their surrounding moats, might provide a source and conduit for fluids to alter the mantle. Alternatively, there may be some mantle deformation process related to the bending that results in the low V_p without a preexisting feature, allowing fluids to more easily alter the oceanic mantle. In either scenario, introduction of fluids into the downgoing mantle could produce serpentine and chlorite, which are stable to high pressures and low temperatures, and have low seismic velocities [*Hacker et al.*, 2003].

7.5. Plate Coupling

[75] The Pacific–North American plate interface is significant because it is the location of seismic slip during great subduction zone earthquakes. The 1964 M_w 9.2 earthquake had a primary asperity, with 15–25 m slip, beneath Prince William Sound and a secondary asperity, with 5–15 m slip, east of Kodiak Island [*Christensen and Beck*, 1994; *Johnson*

et al., 1996]. These two asperities are persistent features in the paleoseismic record [*Combellick*, 1994; *Gilpin*, 1995] that also correspond to current patterns of plate coupling, including the intervening region of low 1964 coseismic slip and near-zero plate coupling (Figure 2a) [*Zweck et al.*, 2002]. The Prince William Sound asperity has very strong coupling ($\geq$1.0) and the Kodiak asperity has moderate coupling (0.4). Strong coupling in the Prince William Sound asperity has been related to the shallow dip and geometric complexity in the region of the Yakutat subduction [*Christensen and Beck*, 1994] and weak coupling has been related to subduction of thick sediments [*von Huene et al.*, 1999].

[76] The location of the Prince William Sound asperity is shown on the cross sections (Figures 9c and 13a), following the strong coupling feature in *Zweck et al.*'s [2002] model. It primarily corresponds to the region of the Yakutat plate, yet it is centered on the southwestern boundary of the Yakutat plate along the Transition fault system (Figures 2a and 2b). This former oblique-slip feature adds significant complexity to the subducting plate, which may have especially thick crust where the Yakutat crust partially overthrusts the Pacific crust. Our results do not address the Kodiak asperity which is near the southern periphery of our study area, where the shallow slab is poorly imaged (Figure 8d).

[77] In the low coseismic-slip region, *Ye et al.* [1997] infer a 20-km-thick underplated low-velocity zone, from forward modeling of the EDGE profile. The 3-D inversion model has a similar velocity reversal at 15-km depth and relatively low velocity above the slab in that area (Figure 8c, x = 0 to −50). *Von Huene et al.* [1999] relate the thick subducted sediment to the zone of weak coupling.

[78] The set of earthquakes selected for velocity inversion have numerous observations and depths that are constrained in single-event locations. Thus the set includes few small-magnitude shallow offshore events. A more comprehensive view of seismicity is provided by *Ratchkovski et al.*'s [2002] double-difference relocations of Prince William Sound seismicity, which are plotted in Figure 13. These used a 1-D velocity model and, for the few common events, they average 6 km shallower than the 3-D hypocenters.

[79] The seismicity is most abundant in the Prince William terrane, both where it is mapped and where it is underthrust below the Chugach terrane (Figure 13). The shallow offshore part of this terrane shows folding and numerous thrusts in seismic reflection profiles [*Plafker*, 1987], and internal deformation throughout the accreting terrane is reasonable. The distributed small earthquakes do not necessarily define significant fault zones, however, they do indicate a broad region of brittle deformation which may include numerous distributed small faults. It is notable that brittle deformation characterizes the entire thickness of the overlying plate, all the way down to the subducting slab. This is also true of the strongly coupled portion of the Hikurangi subduction zone [*Eberhart-Phillips et al.*, 2005]. The western downdip edge of the Prince William Sound asperity is in the vicinity of the Contact fault, which bounds the relatively low-velocity underthrust Prince William terrane. Thus there may be rheological or fluid transport properties of the Prince William terrane that contribute to strong coupling. Alternatively, the terrane boundary may simply coincide with the thermal downdip limit to seismic slip.

[80] The base of seismicity tends to follow the 7.0 km/s contour. This relationship is consistent with the hypothesis of *Brocher et al.* [1994] that the top of the Eocene volcanic crust of the Yakutat terrane may represent a detachment surface. The seismicity and 7 km/s isovelocity contour are relatively flat in the region of the Transition fault and then dip more steeply northwest of the fault. This geometry suggests that the subducting slab is particularly buoyant in the Transition fault region, which is a key factor in producing strong coupling. Thus the localized increase in slab buoyancy associated with the Transition fault, combined with the relatively strong overlying Prince William terrane and relatively low sediment flux, produces the strong Prince William Sound asperity.

7.6. Volcanism/Volcanogenic Subduction

[81] The Cook Inlet volcanoes (y = 0 to 225) lie above a low-V_p, high-V_p/V_s mantle wedge (Figures 8a, 8b, 6e, 6f, 7e, and 7f). In this region, *Kisslinger and Lahr* [1991] observed similar low V_p. In the subduction zone mantle, V_p/V_s is likely elevated by two processes. First, directly beneath the arc volcanoes where melting occurs, the presence of small degrees of partial melt or the hydrating fluids that trigger melting should act to increase V_p/V_s for most expected pore fluid geometries [*Takei*, 2002]. Such anomalies may be seen beneath some volcanoes at 48- to 65-km depth (Figures 7 and 8e). Second, in the shallower parts of the forearc, temperatures can be sufficiently low (<600–700°C) that serpentine is stable, and serpentinite has unusually high V_p/V_s [*Christensen*, 1996]. Attenuation tomography indicates that a transition in wedge temperature happens fairly abruptly above where the slab reaches 80 km depth [*Stachnik et al.*, 2004], so that the shallow, cold part of the mantle wedge is isolated from overall flow [*Kincaid and Sacks*, 1997; *Abers et al.*, 2006]. Such conditions would favor gradual serpentinization as slab-derived fluids migrate up [*Hyndman and Peacock*, 2003; *Brocher et al.*, 2004]. Large wavelength magnetic anomalies beneath the forearc, and high-conductivity lower crustal rocks [*Green*, 2003], also indicate mantle serpentinization through its production of magnetite, and the Alaska magnetic belt [*Blakely et al.*, 2005] corresponds closely to the high-V_p/V_s belt seen at z = 48 km (Figure 7).

[82] At shallow depth (<30 km) we do not image low V_p or high V_p/V_s under the volcanoes, although there could be narrow features such as the 3-km-wide low-V_p conduit observed by *Power et al.* [1998] under Spurr. Underlying Spurr, an extensive region of partial melt below 30 km inferred from high V_p/V_s (Figure 8e) corroborates petrologic investigations that show magma ascends from that depth, rather than residing in the crust [*Power et al.*, 2002]. A similar low V_p, high V_p/V_s is also imaged in Japan in the uppermost mantle beneath many volcanoes [*Nakajima et al.*, 2001].

[83] The upper crustal velocities under the Cook Inlet volcanoes are relatively high (Figures 6b and 6c). They are >6.5 km/s from 6- to 15-km depth, and these velocities are consistent with mafic igneous rock [*Christensen and Mooney*, 1995], which is either associated with the modern arc or its Mesozoic predecessors. Similar velocities typify the modern arc crust in the Aleutians [*Shillington et al.*, 2004].

[84] The Cook Inlet volcanoes are spaced 50 to 80 km apart. The high-V_p/V_s mantle under the Cook Inlet volcanoes is not uniform, but has high-V_p/V_s zones associated with each volcano (Figures 7f and 8e). This variation may reflect lateral variations in the dewatering of the downgoing slab and the resulting hydration of the mantle wedge, or some process that acts to focus melt along strike, such as Rayleigh-Taylor instabilities. For example, *Tamura* [2003] observed distinct fingers of warmer mantle under Japanese volcanoes and deduced a petrological model where partial melt would be preferentially entrained into rising mantle diapirs of hydrous peridotite. In either case, high V_p/V_s probably reflects significant melt present in interconnected cracks or pores [*Takei*, 2002].

[85] The location of Spurr Volcano near the western edge of the subducted Yakutat slab may allow the volcano to tap fluid released by Yakutat subduction, in addition to fluids from underlying Pacific slab subduction. In the section across the Yakutat slab (Figure 8e), the high-V_p/V_s anomaly under Spurr is continuous with the high V_p/V_s in the Yakutat slab. The continuity of high V_p/V_s is also seen in the map views from 65- to 100-km depth (Figure 7). Hence, if the overlying Cretaceous slab prevents vertical Yakutat subduction fluid movement, then alternative movement sublaterally and to the south may be favored. This process would also influence Hayes volcano, a less active volcano north of Spurr.

[86] The inferred sublateral mantle flow is consistent with the anisotropic fast directions determined by *Christensen et al.* [2003] from teleseismic observations on the BEAAR array (Figures 7i and 9b). For ray paths that sample the mantle underlying the subducting slab, the fast direction is northwest, in the dip direction of the slab. However, for ray paths that sample the mantle wedge, the fast direction is southwest, parallel to the strike of the slab. The broadband array did not extend far enough south to discern whether the slab-parallel flow ends at the Cook Inlet. In the North Island of New Zealand, 3-D velocity and anisotropy studies also imply lateral mantle flow containing subduction fluids toward the southern end of the volcanic zone [*Reyners et al.*, 2006]. Mantle anisotropy is related to mantle flow through orientation of olivine [*Nicolas and Christensen*, 1987]. *Kaminski* [2002] showed that mantle flow is still the most likely mechanism when anisotropy is parallel to the slab.

[87] South of Cook Inlet, the Augustine and Katmai volcanoes are also correlated with low-V_p, high-V_p/V_s mantle wedge (Figures 8c and 8d). Here the Aleutian subduction is less oblique, has less complexity of accreted terranes, and is beyond the broad region of the subduction-to-transform transition. The V_p/V_s is particularly high in the shallow part of the mantle wedge overlying the subducting slab from 30- to 60-km depth. Following *Blakely et al.* [2005], this observation may be attributed to dehydration of the downgoing slab in this depth range and to the serpentinization of the forearc upper mantle wedge. The region near Augustine and Katmai has particularly thick subducted sediments [*von Huene et al.*, 1999; *Ye et al.*, 1997]. In subduction systems, *von Huene and Scholl* [1991] show that, despite a significant amount of underplating, the majority of subducted sediment is transported to the mantle where it is recycled through arc magmatism or absorbed into the mantle. Thus the subducted sediment in this region may result in greater amounts of magmatic fluid release.

[88] The Wrangell volcanic field (WVF) lies east of, and is distinctly separate from, the Aleutian volcanoes, and it is located east of the subducted Pacific slab. Mount Wrangell is historically active with minor phreatic eruptions, unlike the major historic eruptions of Cook Inlet volcanoes. Geochemical and petrological analysis shows that the WVF does not contain upper crustal reservoirs of partial melt [*Preece and Hart*, 2004]. Cross sections across the slab show the position of Mount Wrangell relative to the edge of the subducted slab (Figures 10 and 10c). It lies about 50–75 km northeast of the apparent edge of the Yakutat slab (high V_p slab) where the slab is about 50–70 km deep. With the relatively sparse data and coarse inversion grid, we cannot image mantle detail in that region. The V_p/V_s resolution is particularly weak and thus inconclusive. However, the relatively low V_p and moderate V_p/V_s in the lower crust in the region do not rule out a small partial melt zone.

[89] The Wrangell volcanism has been related to Miocene and younger Yakutat subduction [*Plafker and Berg*, 1994]. The northeastern edge of the subducting Yakutat slab reaches about 50-km depth near the Wrangell volcanic field (Figure 10c). The steady dehydration of the subducting slab [*Schmidt and Poli*, 1998] may release fluids which may migrate laterally from the seismogenic slab toward the Wrangell volcanic field. This region northeast of the slab is associated with a high-amplitude magnetic anomaly which *Blakely et al.* [2005] relate to hydration and serpentinization. An edge to the Yakutat slab slightly west of Mount Wrangell has also been deduced through petrological analysis by *Preece and Hart* [2004]. They relate adakites to slab melting induced by asthenospheric mantle flow along the slab edge, analogous to Kamchatka [*Yogodzinski et al.*, 2001].

7.7. Denali Fault

[90] The modern Denali fault is located near a major suture zone between terranes with affinities to the North American continent and accreted terranes [*Nokleberg et al.*, 1985; *Ridgway et al.*, 2002]. *Plafker and Berg* [1994] estimate cumulative post-Cretaceous right-lateral offset to be 140 km on the western part of the fault (west of Mount McKinley) and 400 km on the eastern part of the fault. They infer that the western Denali fault accommodated thrusting during Cretaceous time, as the Kahiltna flysch underthrust the Yukon-Tanana terrane, while strike-slip deformation predominated on the eastern part of the fault.

[91] Currently, the Denali fault is an active strike-slip fault forming the northern boundary of the Wrangell crustal block, which is thought to be extruding westward [*Lahr and Plafker*, 1980; *Haeussler et al.*, 2000]. Geodetic data and cosmogenic dating indicate 8–12 mm/yr right slip on the Denali fault system [*Fletcher*, 2002; *Matmon et al.*, 2004], and the M_w 7.9 earthquake of 3 November 2002 ruptured 240 km of the Denali fault and 115 km on related faults [*Eberhart-Phillips et al.*, 2003].

[92] The Denali fault is prominent in the 3-D velocity model, particularly in the isovelocity plots that indicate variation in crustal thickness (Figure 11). The central Denali fault appears to be a vertical boundary to the depth of

resolution, which is about 50 km (Figures 6f, 10a, and 10b). In the upper 20 km there is little contrast in V_p across the fault, but a greater contrast in V_p/V_s with consistently low V_p/V_s on the north (Figures 7a–7e). These velocity results support the central Denali fault being a plate-bounding lithospheric feature constituting the edge of less deformable North American plate. There is too little resolution to distinguish the eastern Denali fault from the Totschunda fault, but presumably the lithospheric feature continues along the eastern Denali fault and the margin of the Yukon-Tanana terrane. The thickest crust (or lowest velocity mantle) is located at x = 25, where the Denali fault is directly above the edge of the subducted Yakutat slab (Figures 11 and 10a).

[93] The western central Denali fault also appears to be a major crustal feature, and is characterized by low velocity along the fault in the lower crust (west of x = 50 in Figures 6e and 10a). Here BEAAR receiver functions show a 5- to 10-km sharp increase in crustal thickness [*Veenstra et al.*, 2006], which appears to be a more localized feature than for the eastern central Denali fault (Figure 11a). The character of the mantle appears less related to the Denali fault, than for the central fault east of x = 50, since the largest gradient in upper mantle velocities is well south of the fault (Figure 11b). In the region of the subducted Yakutat slab, the western Denali fault is an element of the overlying plate together with the Cretaceous slab and Kahiltna flysch. After closure of the Kahiltna flysch basin, the Denali fault system began accommodating right-lateral strike-slip deformation and appears to have become a subvertical crustal fault. As suggested by *Stanley et al.* [1990], in the ductile crust the fault goes through the underthrust flysch, and thus would partially offset the shallow mapped flysch from the deeper flysch.

[94] The highest topography of the Alaska Range is centered along and south of the western central Denali fault, with Mount McKinley at 6194 m. (Figure 2a), in the area where the Denali fault overlies the deep Yakutat slab. *Ferris et al.* [2003] inferred that the buoyancy of the subducting crust drives mountain building. The buoyancy is illustrated in Figures 10c and 10d. These profiles are essentially parallel to the megathrust, yet as you go to the northeast along the profiles, the depth to the slab gets shallower and shallower. The buoyancy effect would be most pronounced in the central region of the Yakutat slab and this may be seen in the topography. The McKinley region is part of a southeast trending zone of high topography (Figure 2a) which lies above the center (width wise) of the Yakutat slab (Figure 2b). Ultimately the buoyant slab is likely responsible for the deformation far into interior southern Alaska, large-scale mountain building of the Alaska Range and uplift of Mount McKinley.

8. Conclusions

[95] Simultaneous inversion for hypocenters and 3-D V_p and V_p/V_s images the subduction system and broad plate boundary in central Alaska, using local earthquake data, and onland and onshore-offshore active source data. A gradational inversion approach is used, relying on the data to define the structure without including predefined slab structure.

[96] The subducted Pacific plate and mantle wedge are shown, with distinctive properties for the Yakutat slab on the northeast. In the overlying plate, the edge of the North American continental margin terranes is prominent as a lithospheric boundary along the Denali fault that coincides with an approximately 10- to 15-km increase in crustal thickness, with thicker crust to the south in the accreted terranes.

[97] In the crust, low velocity correlates with the Cook Inlet and Copper River basins. High velocity is shown for the metamorphic and mafic intrusive rocks of the Chugach mountains, with a distinct boundary along the Contact fault. The Wrangellia terrane shows relatively high V_p, consistent with mafic arc components, and a boundary is apparent to the low-V_p, low-V_p/V_s Kahiltna flysch terrane. Extending to 65-km depth, the low-V_p, low-resistivity feature represents extensive Cretaceous underthrusting.

[98] Underlying the volcanic systems, high V_p/V_s in the mantle is consistent with partial melt and depths are similar to those inferred petrologically. The high-V_p/V_s mantle under the Cook Inlet volcanoes is not uniform, but has high-V_p/V_s zones associated with each volcano, which may reflect some process that acts to focus melt along strike.

[99] The Yakutat terrane is imaged to 140-km depth as a subducted slab with a thick low-V_p and high-V_p/V_s crust, consistent with an oceanic plateau. The boundary between the subducted Yakutat and Pacific slabs is well defined by velocity and seismicity, and there is no evidence of a tear. Rather than a generic mantle wedge, the subducted Yakutat slab underlies high-velocity material that may represent a Cretaceous subducted slab. This serves to limit vertical mantle flow and volcanism, so that sublateral mantle flow containing subduction fluids is favored toward the Cook Inlet volcanoes.

[100] A distinct northeastern edge is inferred for the Yakutat oceanic slab based on 3-D velocity and seismicity, and is adjacent to a region of >50-km-thick crust. Fluids from the subducting slab may migrate sublaterally toward the Wrangell volcanic field and the slab edge may contribute to adakitic magmas.

[101] The primary asperity of the 1964 M_w 9.2 earthquake, with persistent extremely strong plate coupling, is associated with the southwestern boundary of the Yakutat plate, where the Yakutat crust has partially overthrust the Pacific crust, along the Transition fault system.

[102] The 3-D image of the entire subducted slab constrains interpretation of the surficial Yakutat terrane. In the mantle, we consider that the Yakutat slab is subducting with the Pacific plate and is not moving independently as a truly distinct plate. At shallower depths, as the subducting Pacific plate pulls the more buoyant Yakutat slab downward, the Yakutat slab overthrusts the shallow Pacific plate as a secondary effect. On the basis of the imaged slab geometry, we infer that the Transition fault has long accommodated displacement between the surficial Yakutat terrane and the Pacific plate. Ultimately, the buoyant slab is likely responsible for the deformation far into interior southern Alaska and uplift of Mount McKinley.

[103] **Acknowledgments.** This study builds on numerous data sets collected over nearly 2 decades. We appreciate the hard work of all who deployed instruments, analyzed the traveltimes and maintained databases

for future workers. Specifically, the U.S. Geological Survey (USGS), in collaboration with a number of universities, was primarily responsible for collecting and analyzing the active source data, and the University of Alaska Fairbanks, in collaboration with the USGS, was primarily responsible for collecting and analyzing the earthquake data. We are grateful to Steven Cohen, Diane Doser, Gary Fuis, Stephanie Prejean, and an anonymous referee for their interest and comments, which significantly improved this manuscript. Plots were created using GMT software [*Wessel and Smith*, 1998].

References

Abers, G. A. (2005), Seismic low-velocity layer at the top of subducting slabs beneath volcanic arcs: observations, predictions, and systematics, *Phys. Earth Planet. Inter.*, *149*, 7–29.

Abers, G. A., and G. Sarker (1996), Dispersion of regional body waves at 100–150 km depth beneath Alaska: In situ constraints on metamorphism of subducted crust, *Geophys. Res. Lett.*, *23*, 1171–1174.

Abers, G. A., P. E. van Keken, E. A. Kneller, A. Ferris, and J. C. Stachnik (2006), The thermal structure of subduction zones constrained by seismic imaging: Slab dehydration and wedge flow, *Earth Planet. Sci. Lett.*, *241*, 387–397.

Akaogi, M., H. Yusa, K. Shiraishi, and T. Suzuki (1995), Thermodynamic properties of alpha quartz, coesite and stishovite and equilibrium phase-relations at high-pressures and high-temperatures, *J. Geophys. Res.*, *100*, 22,337–22,347.

Beaudoin, B. C. (1994), Lower-crustal deformation during terrane dispersion along strike-slip faults, *Tectonophysics*, *232*, 257–266.

Beaudoin, B. C., G. S. Fuis, W. D. Mooney, W. J. Nokleberg, and N. I. Christensen (1992), Thin, low-velocity crust beneath the southern Yukon-Tanana terrane, east-central Alaska: Results from Trans-Alaska Crustal Transect refraction/wide-angle reflection data, *J. Geophys. Res.*, *97*, 1921–1942.

Behn, M. D., and P. B. Kelemen (2003), Relationship between seismic P-wave velocity and the composition of anhydrous igneous and meta-igneous rocks, *Geochem. Geophys. Geosyst.*, *4*(5), 1041, doi:10.1029/2002GC000393.

Blakely, R. J., T. M. Brocher, and R. E. Wells (2005), Subduction zone magnetic anomalies and implications for hydrated forearc mantle, *Geology*, *33*, 445–448.

Bol, A. J., and H. Gibbons (1992), Tectonic implications of out-of-sequence faults in an accretionary prism, Prince William Sound, Alaska, *Tectonics*, *11*, 1288–1300.

Bol, A. J., and S. M. Roeske (1993), Strike-slip faulting and block rotation along the Contact fault system, eastern Prince William Sound, Alaska, *Tectonics*, *12*, 49–62.

Brocher, T. M., and M. J. Moses (1990), Wide-angle seismic recordings obtained during the TACT multichannel reflection profiling in the northern Gulf of Alaska, *U.S. Geol. Surv. Open File Rep.*, *90-663*, 40 pp.

Brocher, T. M., and M. J. Moses (1993), Onshore-offshore wide-angle seismic recordings of the 1989 Alaskan EDGE profile: Five-day recorder data, *U.S. Geol. Surv. Open File Rep.*, *93-238*, 25 pp.

Brocher, T. M., M. A. Fisher, E. L. Geist, and N. I. Christensen (1989), A high-resolution reflection/refraction study of the Chugach-Peninsular terrane boundary, southern Alaska, *J. Geophys. Res.*, *94*, 4441–4455.

Brocher, T. M., W. J. Nokleberg, N. I. Christensen, W. J. Lutter, E. L. Geist, and M. A. Fisher (1991), Seismic reflection/refraction mapping of faulting and regional dips in the eastern Alaska Range, *J. Geophys. Res.*, *96*, 10,233–10,249.

Brocher, T. M., G. S. Fuis, M. A. Fisher, G. Plafker, M. J. Moses, J. J. Taber, and N. I. Christensen (1994), Mapping the megathrust beneath the northern Gulf of Alaska using wide-angle seismic data, *J. Geophys. Res.*, *99*, 11,663–11,685.

Brocher, T. M., T. Parsons, A. M. Trèhu, C. M. Snelsom, and M. A. Fisher (2003), Seismic evidence for widespread serpentinized forearc upper mantle along the Cascadia margin, *Geology*, *31*, 267–270.

Brocher, T. M., G. S. Fuis, W. J. Lutter, N. I. Christensen, and N. A. Ratchkovski (2004), Seismic velocity models for the Denali fault zone along the Richardson Highway, Alaska, *Bull. Seismol. Soc. Am.*, *94*, S85–S106.

Bruhn, R. L., W. T. Parry, and M. P. Bunds (2000), Tectonics, fluid migration, and fluid pressure in a deformed forearc basin, Cook Inlet, Alaska, *Geol. Soc. Am. Bull.*, *112*, 550–563.

Bruhn, R. L., T. L. Pavlis, G. Plafker, and L. Serpa (2004), Deformation during terrane accretion in the Saint Elias orogen, Alaska, *Geol. Soc. Am. Bull.*, *116*, 771–787.

Bruns, T. R. (1983), Model for the origin of the Yakutat block, an accreted terrane in the northern Gulf of Alaska, *Geology*, *11*, 718–721.

Buland, R., and C. H. Chapman (1983), The computation of seismic travel times, *Bull. Seismol. Soc. Am.*, *73*, 1271–1301.

Christensen, D. H., and S. L. Beck (1994), The rupture process and tectonic implications of the great 1964 Prince William Sound earthquake, *Pure Appl. Geophys.*, *142*, 29–53.

Christensen, D. H., G. A. Abers, and T. L. McKnight (2003), Mantle anisotropy beneath the Alaska range inferred from S-wave splitting observations: Results from BEAAR, *Eos Trans. AGU*, *84*(46), Fall Meet. Suppl., Abstract S31C-0782.

Christensen, N. I. (1996), Poisson's ratio and crustal seismology, *J. Geophys. Res.*, *101*, 3139–3156.

Christensen, N. I., and W. D. Mooney (1995), Seismic velocity structure and composition of the continental crust: A global view, *J. Geophys. Res.*, *100*, 9761–9788.

Combellick, R. A. (1994), Investigations of peat stratigraphy in tidal marshes along Cook Inlet, Alaska, to determine the frequency of 1964-style great earthquakes in the Anchorage region, *Rep. of Invest. 94-7*, pp. 24, Alaska Dep. of Nat. Resour., Div. of Geol. and Geophys. Surv., Fairbanks.

DeBari, S. M., and N. H. Sleep (1991), High-Mg, low-Al bulk composition of the Talkeetna Island Arc, Alaska—Implications for primary magmas and the nature of arc crust, *Geol. Soc. Am. Bull.*, *103*, 37–47.

DeMets, C., R. G. Gordon, D. F. Argus, and S. Stein (1994), Effect of recent revisions to the geomagnetic reversal timescale on estimates of current plate motions, *Geophys. Res. Lett.*, *21*, 2191–2194.

Doser, D. I., and W. A. Brown (2001), A study of historic earthquake of the Prince William Sound, Alaska region, *Bull. Seismol. Soc. Am.*, *91*, 842–857.

Doser, D. I., and R. Lomas (2000), The transition from strike-slip to oblique subduction in the southeastern Alaska from seismological studies, *Tectonophysics*, *316*, 45–65.

Doser, D. I., J. R. Pelton, and A. M. Veilleux (1997), Earthquakes in the Pamplona zone, Yakutat Block, south central Alaska, *J. Geophys. Res.*, *102*, 24,449–24,511.

Doser, D. I., A. Veilleux, and M. Velasquez (1999), Seismicity of the Prince William Sound region for thirty two years following the 1964 Great Alaskan earthquake, *Pure Appl. Geophys.*, *154*, 593–632.

Dumoulin, J. A. (1988), Sandstone petrographic evidence and the Chugach-Prince William terrane boundary in southern Alaska, *Geology*, *15*, 456–460.

Eberhart-Phillips, D. (1986), Three-dimensional velocity structure in northern California coast ranges from inversion of local earthquake arrival times, *Bull. Seismol. Soc. Am.*, *76*, 1025–1052.

Eberhart-Phillips, D. (1990), Three-dimensional P- and S-velocity structure in the Coalinga region, California, *J. Geophys. Res.*, *95*, 15,343–15,363.

Eberhart-Phillips, D. (1993), Local earthquake tomography: Earthquake source regions, in *Seismic Tomography: Theory and Practice*, edited by H. M. Iyer and K. Hirahara, pp. 613–643, CRC Press, Boca Raton, Fla.

Eberhart-Phillips, D., and S. Bannister (2002), Three-dimensional crustal structure in the Southern Alps region of New Zealand from inversion of local earthquake and active source data, *J. Geophys. Res.*, *107*(B10), 2262, doi:10.1029/2001JB000567.

Eberhart-Phillips, D., and A. J. Michael (1998), Seismotectonics of the Loma Prieta, California, region determined from three-dimensional Vp, Vp/Vs, and seismicity, *J. Geophys. Res.*, *103*, 21,099–21,120.

Eberhart-Phillips, D., et al. (2003), The 2002 Denali fault earthquake, Alaska: A large magnitude, slip-partitioned event, *Science*, *300*, 1113–1118.

Eberhart-Phillips, D., M. Reyners, M. Chadwick, and J.-M. Chiu (2005), Crustal heterogeneity and subduction processes: 3-D Vp, Vp/Vs and Q in the southern North Island, New Zealand, *Geophys. J. Int.*, *162*, 270–288.

Ehm, A. (1983), Oil and gas basins map of Alaska, Alaska Dep. of Nat. Resour., Juneau.

Estabrook, C. H., J. L. Nabelek, and A. L. Lerner–Lam (1992), Tectonic model of the Pacific North American plate boundary in the Gulf of Alaska from broadband analysis of the 1979 St. Elias, Alaska, earthquake and its aftershocks, *J. Geophys. Res.*, *97*, 6587–6612.

Ferris, A., G. A. Abers, D. H. Christensen, and E. Veenstra (2003), High resolution image of the subducted Pacific (?) plate beneath central Alaska, 50–150 km depth, *Earth Planet. Sci. Lett.*, *214*, 575–588.

Fisher, M. A., R. V. Huene, G. L. Smith, and T. R. Bruns (1983), Possible seismic reflections from the downgoing Pacific plate, 275 kilometers arcward of the eastward Aleutian Trench, *J. Geophys. Res.*, *88*, 5835–5849.

Fisher, M. A., T. M. Brocher, W. J. Nokleberg, G. Plafker, and G. L. Smith (1989), Seismic reflection images of the crust of the northern part of the Chugach terrane, Alaska: Results of a survey for the Trans-Alaska Crustal Transect (TACT), *J. Geophys. Res.*, *94*, 4424–4440.

Fisher, M. A., N. A. Ratchkovski, W. J. Nokleberg, L. Pellerin, and J. M. G. Glen (2004), Geophysical data reveal the crustal structure of the Alaska Range orogen within the aftershock zone of the M_w 7.9 Denali fault earthquake, *Bull. Seismol. Soc. Am.*, *94*, S107–S131.

Fisher, M. A., N. A. Ruppert, D. M. Eberhart-Phillips, T. M. Brocher, R. E. Wells, R. J. Blakely, and R. W. Sliter (2005), Tectonics and seismicity of the Alaskan continental margin near the collision zone of the Yakutat Terrane and the epicenter of the 1964 great Alaska earthquake, *Geol. Soc. Am. Abstr. Programs*, *37*, 79.

Fitzgerald, P. G., R. B. Sorkhabi, T. F. Redfield, and E. Stump (1995), Uplift and denudation of the central Alaska Range: A case study in the use of apatite fission track thermochronology to determine absolute uplift parameters, *J. Geophys. Res.*, *100*, 20,175–20,191.

Fletcher, H. J. (2002), Tectonics in interior Alaska from GPS measurements, Ph.D. thesis, 257 pp., Univ. of Alaska, Fairbanks.

Fletcher, H. J., and J. T. Freymueller (1999), New GPS constrains on the motion of the Yakutat block, *Geophys. Res. Lett.*, *26*, 3029–3032.

Fletcher, H. J., and J. T. Freymueller (2003), New constraints on the motion of the Fairweather fault, Alaska, from GPS observations, *Geophys. Res. Lett.*, *30*(3), 1139, doi:10.1029/2002GL016476.

Flueh, E. R., W. D. Mooney, G. S. Fuis, and E. L. Ambos (1989), Crustal structure of the Chugach Mountains, southern Alaska: A study of peg-leg multiples from a low-velocity zone, *J. Geophys. Res.*, *94*, 16,023–16,035.

Frost, G. M., D. F. Barnes, and R. G. Stanley (2002), Geologic and isostatic gravity map of the Nenana Basin Area, central Alaska, *U.S. Geol. Surv. Geol. Invest. Ser.*, *I-2543*.

Fuis, G. S., and G. Plafker (1991), Evolution of deep structure along the Trans-Alaska Crustal Transect, Chugach Mountains and Copper River Basin, southern Alaska, *J. Geophys. Res.*, *96*, 4229–4253.

Fuis, G. S., E. L. Ambos, W. D. Mooney, N. I. Christensen, and E. L. Geist (1991), Crustal structure of accreted terranes in southern Alaska, Chugach Mountains and Copper River Basin, from seismic refraction results, *J. Geophys. Res.*, *96*, 4187–4227.

Fuis, G. S., J. M. Murphy, W. J. Lutter, T. E. Moore, K. J. Bird, and N. I. Christensen (1997), Deep seismic structure and tectonics of northern Alaska: Crustal-scale duplexing with deformation extending into the upper mantle, *J. Geophys. Res.*, *102*, 20,873–20,896.

Gerbault, M., F. J. Davey, and S. Henrys (2002), Three-dimensional lateral crustal thickening in continental oblique collision: An example from the Southern Alps, New Zealand, *Geophys. J. Int.*, *150*, 770–779.

Gilpin, L. M. (1995), Holocene paleoseismicity and coastal tectonics of the Kodiak Islands, Alaska, Ph.D. thesis, Univ. of Calif., Santa Cruz.

Goodwin, E. B., G. S. Fuis, W. J. Nokleberg, and E. L. Ambos (1989), The crustal structure of the Wrangellia terrane along the East Glenn Highway, eastern-southern Alaska, *J. Geophys. Res.*, *94*, 16,037–16,057.

Green, A. M. (2003), Magnetotelluric crustal studies in Kenai, Alaska, M.S. thesis, Colo. Sch. of Mines, Golden.

Hacker, B. R. (1996), Eclogite formation and the rheology, buoyancy, seismicity, and H_2O content of oceanic crust, in *Subduction: Top to Bottom*, *Geophys. Monogr. Ser.*, vol. 96, edited by G. E. Bebout et al., pp. 337–346, AGU, Washington, D. C.

Hacker, B. R., G. A. Abers, and S. M. Peacock (2003), Subduction factory: 1. Theoretical mineralogy, densities, seismic wave speeds, and H_2O contents, *J. Geophys. Res.*, *108*(B1), 2029, doi:10.1029/2001JB001127.

Haeussler, P. J., R. L. Bruhn, and T. L. Pratt (2000), Potential seismic hazards and tectonics of the upper Cook inlet basin, Alaska, based on analysis of Pliocene and younger deformation., *Geol. Soc. Am. Bull.*, *112*, 1414–1429.

Hyndman, R. D., and S. M. Peacock (2003), Serpentinization of the forearc mantle, *Earth Planet. Sci. Lett.*, *212*, 417–432.

Johnson, J. M., K. Satake, S. R. Holdahl, and J. Sauber (1996), The 1964 Prince William Sound earthquake: Joint inversion of tsunami and geodetic data, *J. Geophys. Res.*, *101*, 523–532.

Kaminski, E. (2002), The influence of water on the development of lattice preferred orientation in olivine aggregates, *Geophys. Res. Lett.*, *29*(12), 1576, doi:10.1029/2002GL014710.

Kennett, B. L. N., and E. R. Engdahl (1991), Travel times for global earthquake location and phase identification, *Geophys. J. Int.*, *105*, 429–465.

Kincaid, C., and I. S. Sacks (1997), Thermal and dynamical evolution of the upper mantle in subduction zones, *J. Geophys. Res.*, *102*, 12,295–12,315.

Kirschner, C. E., and C. A. Lyon (1973), Stratigraphic and tectonic development of Cook Inlet petroleum province, in *Arctic Geology, Proceedings*, edited by M. G. Pitcher, *AAPG Mem.*, *19*, 396–407.

Kisslinger, E., and J. C. Lahr (1991), Tomographic image of the Pacific slab under southern Alaska, *Eclogae Geol. Helv.*, *84*, 297–315.

Kohler, M. D., and D. Eberhart-Phillips (2003), Intermediate-depth earthquakes in a region of continental convergence: South Island, New Zealand, *Bull. Seismol. Soc. Am.*, *93*, 85–93.

Lahr, J. C., and G. Plafker (1980), Holocene Pacific-North American plate interaction in southern Alaska: Implications for the Yakataga seismic gap, *Geology*, *8*, 483–486.

Levander, A., G. S. Fuis, E. S. Wissinger, W. J. Lutter, J. S. Oldow, and T. E. Moore (1994), Seismic images of the Brooks Range fold and thrust belt, Arctic Alaska, from an intergrated seismic reflection/refraction experiment, *Tectonophysics*, *232*, 13–30.

Liou, J. G., R. Y. Zhang, W. G. Ernst, D. Rumble, and S. Maruyama (1998), High-pressure minerals from deeply subducted metamorphic rocks, in *Ultrahigh Pressure Mineralogy: Physics and Chemistry of Earth's Deep Interior*, *Rev. Mineral.*, vol. 37, edited by R. Hemley and D. Mao, pp. 33–96, Mineral. Soc. of Am., Washington, D. C.

Matmon, A., D. Schwartz, H. Stenner, J. Lienkamper, T. Dawson, P. J. Haeussler, L. Staft, and R. C. Finkel (2004), Determining Holocene and late Pleistocene slip rates along the Denali Fault using cosmogenic ^{10}Be analysis of boulders on displaced moraines, paper presented at 2004 Annual Meeting, Geol. Soc. of Am., Denver, Colo.

McNamara, D. E., and M. E. Pasyanos (2002), Seismological evidence for a sub-volcanic arc mantle wedge beneath the Denali volcanic gap, Alaska, *Geophys. Res. Lett.*, *29*(16), 1814, doi:10.1029/2001GL014088.

Michelini, A., and T. V. McEvilly (1991), Seismological studies at Parkfield: I. Simultaneous inversion for velocity structure and hypocenters using cubic b-splines parameterization, *Bull. Seismol. Soc. Am.*, *81*, 524–552.

Miller, T. P., and D. H. Richter (1994), Quaternary volcanism in the Alaska Peninsula and Wrangell Mountains, Alaska, in *The Geology of Alaska*, edited by G. Plafker and H. C. Berg, pp. 759–779, Geological Society of America, Boulder, Colo.

Molnar, P., and H. Lyon-Caen (1988), Some simple physical aspects of the support, structure, and evolution of mountain belts, in *Processes in Continental Lithospheric Deformation*, edited by S. P. Clark, *Spec. Pap. Geol. Soc. Am.*, *218*, 179–207.

Mooney, W. D., G. Laske, and G. Masters (1998), CRUST 5.1: A global crustal model at $5^\circ \times 5^\circ$, *J. Geophys. Res.*, *103*, 727–747.

Moore, J. C., et al. (1991), EDGE deep seismic reflection transect of the eastern Aleutian arc-trench layered lower crust reveals underplanting and continental growth, *Geology*, *19*, 420–424.

Nakajima, J., T. Matsuzawa, A. Hasegawa, and D. Zhao (2001), Three-dimensional structure of Vp, Vs, and Vp/Vs beneath northeastern Japan: Implications for arc magmatism and fluids, *J. Geophys. Res.*, *106*, 21,843–21,857.

Nicolas, A., and N. I. Christensen (1987), Formation of anisotropy in upper mantle peridotites: A review, in *Composition, Structure and Dynamics of the Lithosphere-Asthenosphere System*, *Geodyn. Ser.*, vol. 16, edited by K. Fuchs and C. Froidevaux, pp. 111–123, AGU, Washington, D. C.

Nokleberg, W. J., D. L. Jones, and N. J. Siberling (1985), Origin and tectonic evolution of the Maclaren and Wrangellia terranes, eastern Alaska Range, Alaska, *Geol. Soc. Am. Bull.*, *96*, 1251–1270.

Nokleberg, W. J., H. L. Foster, and J. N. Aleinikoff (1989), Geology of the northern Copper River basin, eastern Alaska Range, and southern Yukon-Tanana Basin, southern and east-central Alaska, in *Sedimentation and Tectonics of Western North America*; vol. 1, *Alaskan Geological and Geophysical Transect*, *Field Trip Guideb.*, vol. T104, edited by W. J. Nokleberg and M. A. Fisher, pp. 34–63, AGU, Washington, D. C.

Nokleberg, W. J., L. M. Parfenov, J. W. H. Monger, I. O. Norton, A. I. Khanchuk, D. B. Stone, D. W. Scholl, and K. Fujita (2000), Phanerozoic tectonic evolution of the Circum-North Pacific, *U.S. Geol. Surv. Prof. Pap., 1626*, 122 pp.

Nye, C. J. (1999), The Denali volcanic gap—Magmatism at the eastern end of the Aleutian Arc, *Eos Trans. AGU*, *80*(46), Fall Meet. Suppl., F1202.

Page, R. A., C. D. Stephens, and J. C. Lahr (1989), Seismicity of the Wrangell and Aleutian Wadati-Benioff zones and the North American plate along the Trans-Alaska Crustal Transect, Chugach Mountains and Copper River Basin, southern Alaska, *J. Geophys. Res.*, *94*, 16,059–16,082.

Pavlis, T. L., C. Picornell, L. Serpa, R. L. Bruhn, and G. Plakfker (2004), Tectonic processes during oblique convergence: Insights from the St. Elias Orogen, northern North American Cordillera, *Tectonics*, *23*, TC3001, doi:10.1029/2003TC001557.

Plafker, G. (1987), Regional geology and petroleum potential of the northern Gulf of Alaska continental margin, in *Geology and Resource Potential of the Continental Margin of Western North America and Adjacent Ocean Basins—Beaufort Sea to Baja California*, *Earth Sci. Ser.*, vol. 6, edited by D. W. Scholl, A. Grantz, and J. G. Vedder, pp. 229–268, Circum-Pac. Counc. for Energy and Miner. Resour., Houston, Tex.

Plafker, G., and H. C. Berg (1994), Overview of the geology and tectonic evolution of Alaska, in *The Geology of North America*, vol. G-1, *The Geology of Alaska*, edited by G. Plafker and H. C. Berg, pp. 989–1021, Geol. Soc. of Am., Boulder, Colo.

Plafker, G., J. C. Moore, and G. R. Winkler (1994a), Geology of the southern Alaska margin, in *The Geology of North America*, vol. G-1, *The Geology of Alaska*, edited by G. Plafker and H. C. Berg, pp. 389–449, Geol. Soc. of Am., Boulder, Colo.

Plafker, G., L. M. Gilpin, and J. C. Lahr (1994b), Neotectonic map of Alaska, in *The Geology of North America*, vol. G-1, *The Geology of Alaska*, edited by G. Plafker and H. C. Berg, plate 12, Geol. Soc. of Am., Boulder, Colo.

Power, J. A., A. Villasenor, and H. M. Benz (1998), Seismic image of the Mount Spurr magmatic system, *Bull. Volcanol.*, *60*, 27–37.

Power, J. A., A. D. Jolly, C. J. Nye, and M. L. Harbin (2002), A conceptual model of the Mount Spurr magmatic system from seismic and geochemical observations of the 1992 Crater Peak eruption sequence, *Bull. Volcanol.*, *64*, 206–218.

Preece, S. J., and W. K. Hart (2004), Geochemical variations in the <5 Ma Wrangell volcanic field, Alaska: Implications for the magmatic and tectonic development of a complex continental arc system, *Tectonophysics*, *392*, 165–191.

Pulpan, H., and C. Frohlich (1985), Geometry of the subducted plate near Kodiak Island and lower Cook Inlet, Alaska, determined from relocated earthquake hypocenters, *Bull. Seismol. Soc. Am.*, *75*, 791–810.

Pysklywec, R. N., C. Beaumont, and P. Fullsack (2002), Lithospheric deformation during the early stages of continental collision: Numerical experiments and comparison with South Island, New Zealand, *J. Geophys. Res.*, *107*(B7), 2133, doi:10.1029/2001JB000252.

Ratchkovski, N. A., and R. A. Hansen (2002), New evidence for segmentation of the Alaska subduction zone, *Bull. Seismol. Soc. Am.*, *92*, 1754–1765.

Ratchkovski, N. A., J. Pujol, and N. Biswas (1997), Stress pattern in the double seismic zone beneath Cook Inlet, south-central Alaska, *Tectonopysics*, *281*, 163–172.

Ratchkovski, N. A., J. Pujol, and N. Biswas (1998), Relocation of shallow earthquakes in southern Alaska using joint hypocenter determination method, *J. Seismol.*, *2*, 87–102.

Ratchkovski, N. A., R. A. Hansen, and J. T. Freymueller (2002), What can we learn from the double-difference relocations of the Alaska earthquake catalog?, *Eos Trans. AGU*, *83*(47), Fall Meet. Suppl., Abstract S22B-1014.

Ratchkovski, N. A., et al. (2003), Aftershock sequence of the M_w 7.9 Denali, Alaska, earthquake of 3 November 2002 from regional seismic net work data, *Seismol. Res. Lett.*, *74*, 743–752.

Reed, B. L., and M. A. Lanphere (1973), Alaska-Aleutian Range batholith; Geochronology, chemistry, and relation to circum-Pacific plutonism, *Geol. Soc. Am. Bull.*, *84*, 2583–2609.

Reyners, M., D. Eberhart-Phillips, and G. Stuart (1999), A three-dimensional image of shallow subduction: Crustal structure of the Raukumara Peninsula, New Zealand, *Geophys. J. Int.*, *137*, 873–890.

Reyners, M., D. Eberhart-Phillips, G. Stuart, and Y. Nishimura (2006), Imaging subduction from the trench to 300 km depth beneath the central North Island, New Zealand, with Vp and Vp/Vs, *Geophys. J. Int.*, *165*, 565–583.

Richter, D., and N. Matson (1971), Quaternary faulting in the eastern Alaska Range, *Geol. Soc. Am. Bull.*, *82*, 1529–1539.

Richter, D. H., J. G. Smith, M. A. Lanphere, G. B. Dalrymple, B. L. Reed, and N. Shew (1990), Age and progression of volcanism, Wrangell volcanic field, Alaska, *Bull. Volcanol.*, *53*, 29–44.

Ridgway, K. D., J. M. Trop, W. J. Nokleberg, C. M. Davidson, and K. R. Eastham (2002), Mesozoic and Cenozoic tectonics of the eastern and central Alaska Range: Progressive basin development and deformation in a suture zone, *Geol. Soc. Am. Bull.*, *114*, 1480–1504.

Rossi, G., G. A. Abers, S. Rondenay, and D. H. Christensen (2006), Unusual mantle Poisson's ratio, subduction and crustal structure in central Alaska, *J. Geophys. Res.*, *111*, B09311, doi:10.1029/2005JB003956.

Rudnick, R. L., and D. M. Fountain (1995), Nature and composition of the continental crust: A lower crustal perspective, *Rev. Geophys.*, *33*, 267–309.

Schmidt, M. W., and S. Poli (1998), Experimentally based water budgets for dehydrating slabs and consequences for arc magma generation, *Earth Planet. Sci. Lett.*, *163*, 361–379.

Searcy, C. K. (1996), Crustal and upper mantle velocity structure in Alaska, Ph.D. thesis, 145 pp., Univ. of Alaska, Fairbanks.

Searcy, C. K., D. H. Christensen, and G. Zandt (1996), Velocity structure beneath College Station, Alaska (COL), from inversion of receiver functions, *Bull. Seismol. Soc. Am.*, *86*, 232–241.

Shillington, D., H. J. A. Van Avendonk, W. S. Holbrook, P. B. Kelemen, and M. J. Hornbach (2004), Composition and structure of the central Aleutian Island arc from arc-parallel wide-angle seismic data, *Geochem. Geophys. Geosyst.*, *5*, Q10006, doi:10.1029/2004GC000715.

Silver, E. A., R. von Huene, and J. K. Crouch (1974), Tectonic significance of the Kodiak-Bowie seamount chain, northeastern Pacific, *Geology*, *2*, 147–150.

Stachnik, J. C., G. A. Abers, and D. H. Christensen (2004), Seismic attenuation and mantle wedge temperatures in the Alaska subduction zone, *J. Geophys. Res.*, *109*, B10304, doi:10.1029/2004JB003018.

Stanley, W. D., V. F. Labson, W. J. Nokleberg, B. J. Csejtey, and M. A. Fisher (1990), The Denali fault system and Alaska Range of Alaska: Evidence for underplated Mesozoic flysch from magnetotelluric surveys, *Geol. Soc. Am. Bull.*, *102*, 160–173.

Stephens, C. D., K. A. Fogelman, J. C. Lahr, and R. A. Page (1984), Wrangell Benioff zone southern Alaska, *Geology*, *12*, 373–376.

Stock, J. M., and P. Molnar (1988), Uncertainties and implications of the late Cretaceous and Tertiary position of North America relative to the Farallon, Kula, and Pacific plates, *Tectonics*, *7*, 1339–1384.

Stone, D. B., R. A. Page, and J. N. Davies (1986), Trans-Alaska Lithosphere Investigation: Program prospectus, *U.S. Geol. Surv. Circ.*, *C0984*, 24 pp.

Takei, Y. (2002), Effect of pore geometry on Vp/Vs: From equilibrium geometry to crack, *J. Geophys. Res.*, *107*(B2), 2043, doi:10.1029/2001JB000522.

Tamura, Y. (2003), Some geochemical constraints on hot fingers in the mantle wedge: Evidence from NE Japan, in *Intra-oceanic Subduction Systems: Tectonic and Magmatic Processes*, edited by R. D. Larter and P. T. Leat, pp. 221–237, Geol. Soc. London, London, U. K.

Thurber, C. H. (1983), Earthquake locations and three-dimensional crustal structure in the Coyote Lake area, central California, *J. Geophys. Res.*, *88*, 8226–8236.

Thurber, C. H. (1993), Local earthquake tomography: Velocities and Vp/Vs—Theory, in *Seismic Tomography: Theory and Practice*, edited by H. M. Iyer and K. Hirahara, pp. 563–583, CRC Press, Boca Raton, Fla.

van Wormer, J. D., J. Davies, and L. Gedney (1974), Seismicity and plate tectonics in south central Alaska, *Bull. Seismol. Soc. Am.*, *64*, 1467–1475.

Veenstra, E., D. Christensen, G. A. Abers, and A. Ferris (2006), Crustal thickness variation in south central Alaska: Results from the Broadband Experiment Across the Alaska Range, *Geology*, *34*, 781–784.

von Huene, R., and D. W. Scholl (1991), Observations at convergent margins concerning sediment subduction, subduction erosion, and the growth of continental crust, *Rev. Geophys.*, *29*, 279–316.

von Huene, R., D. Klaeschen, and J. Fruehn (1999), Relation between the subducting plate and seismicity associated with the great 1964 Alaska earthquake, *Pure Appl. Geophys.*, *154*, 575–591.

Wagner, L. S., S. Beck, and G. Zandt (2005), Upper mantle structure in the south central Chilean subduction zone (30° to 36°S), *J. Geophys. Res.*, *110*, B01308, doi:10.1029/2004JB003238.

Wessel, P., and W. H. F. Smith (1998), New version of the generic mapping tools released, *Eos Trans. AGU*, *79*, 579.

Wiemer, S., and M. Wyss (2000), Minimum magnitude of completeness in earthquake catalogs: Examples from Alaska, the western United States and Japan, *Bull. Seismol. Soc. Am.*, *90*, 859–869.

Wolf, L. W., D. B. Stone, and J. N. Davies (1991), Crustal structure of the active margin, south central Alaska: An interpretation of seismic refraction data from the Trans-Alaska Crustal Transect, *J. Geophys. Res.*, *96*, 16,455–16,469.

Ye, S., E. R. Flueh, D. Klaeschen, and R. von Huene (1997), Crustal structure along the EDGE transect beneath the Kodiak Shelf off Alaska derived from OBH seismic refractions data, *Geophys. J. Int.*, *130*, 283–302.

Yogodzinski, G. M., J. M. Lees, T. G. Churikova, F. Dorendorf, G. Woerner, and O. N. Volynets (2001), Geochemical evidence for the melting of subducting oceanic lithosphere at plate edges, *Nature*, *409*, 500–504.

Zhao, D., D. H. Christensen, and H. Pulpan (1995), Tomographic imaging of the Alaska subduction zone, *J. Geophys. Res.*, *100*, 6487–6504.

Zweck, C., J. T. Freymueller, and S. C. Cohen (2002), Three-dimensional dislocation modeling of the postseismic response to the 1964 Alaska earthquake, *J. Geophys. Res.*, *107*(B4), 2064, doi:10.1029/2001JB000409.

G. A. Abers, Department of Earth Sciences, Boston University, 685 Commonwealth Ave., Boston, MA 02215, USA.

T. M. Brocher, U.S. Geological Survey, 345 Middlefield Rd MS 977, Menlo Park, CA 94025-3591, USA.

D. H. Christensen, R. Hansen, and N. A. Ruppert, Geophysical Institute, University of Alaska, P.O. Box 757320, Fairbanks, AK 99775-7320, USA.

D. Eberhart-Phillips, Institute of Geological and Nuclear Sciences, Private Bag 1930, Dunedin, 9020, New Zealand. (d.eberhart@gns.cri.nz)

P. J. Haeussler, U.S. Geological Survey, 4200 University Dr., Anchorage, AK 99508-4667, USA.